UNIVERSITAT POLITÈCNICA DE CATALUNYA
BARCELONATECH
Escola d'Enginyeria de Barcelona Est

MASTER'S THESIS

Master's Degree in Chemical Engineering

SEPARATION AND RECOVERY OF METALS FROM ACIDIC MINE WATERS BY ION EXCHANGE RESINS

Report

Author: Carlos Solís García
Director: José Luis Cortina Pallas
Co-Director: Xanel Vecino Bello

Date: June 2018

Abstract

Mining industry is the major producer of acidic sulphur-rich effluents, which often contain elevated concentrations of heavy metals (e.g. Cd, Cr, Hg, Ni, Pb, Cu, Zn, among others), and non-metals (e.g. As, Se). The most widespread method used to mitigate acidic effluents is an active treatment involving a chemical-neutralizing agent to raise water's pH, causing the precipitation as hydroxides and carbonates of many of the metals present in solution. After this, sludge rich in metals are obtained. Although chemical treatment can provide effective remediation of acidic mine drainage, it has disadvantages of high operating costs and sludge disposal problems. Therefore, as prices for several valuable metals (e.g. zinc and copper) are increasing over the last years, the main objective of this project is to separate and recover rich streams in Zn and Cu by means of ion-exchange resins, using batch and columns systems, from mining effluents. At the end, by the use of electrochemical treatments, like electrowinning, will be used to valorise individually Zn and Cu taking the advantage of the different electrical potentials for their reduction. The treatment scheme provides a circular economy approach for sulphide and coal mining and for metallurgical processing plants.

Some experiments will be conducted by batch and columns set-ups, samples obtained will be analysed by equipment based on different analytic techniques (Atomic Absorption Spectrometry (AAS), Inductively Coupled Plasma (ICP), Field-emission Scanning Electron Microscopy (FESEM), among others). Produced streams rich in Zn or Cu will be characterized and data will be used to determine the process efficiency and the metal recovery ratios.

Firstly, a chemical neutralization treatment will be applied as a pretreatment to eliminate iron(III) and aluminum(III) from acidic mine waters. As iron is typically found as mixtures of Fe(II) and Fe(III) it will be needed to be oxidized quantitatively to Fe(III) After that, experiments will be carried out in batch mode to determine the ion selectivity and extraction curves of ion-exchange resins having different functional groups. Lewatit TP 207 as a chelating ion-exchange resin, and solvent-impregnated ion-exchange resins (SIRs) such as Lewatit VP OC 1026 and Lewatit TP 272 will be evaluated.

Following batch set-up, column tests will be carried out in order to determine breakthrough and elution curves to determine the operation cycle parameters as well as the concentration factor resulting of the ion-exchange step. The last step of the study will include batch operation in an electrolytic cell in order to study the parameters involved in Cu and Zn deposition, such as applied current intensity and pH.

Acknowledgements

This research was supported by the Waste2Product project (CTM2014-57302-R) and by R2MIT project (CTM2017-85346-R) financed by the Spanish Ministry of Economy and Competitiveness (MINECO) and the Catalan Government (ref. 2017-SGR-312), Spain.

Firstly, I would like to express my gratitude to my director Prof. José Luis Cortina for offering me the chance to work in this project and develop the present Master's Thesis in the same field. In addition, my most sincere thanks to Dr. Xanel Bello Vecino, who co-directed and supervised this work, together with Dr. Mònica Reig i Amat. For their patience after many long hours and several additional issues, but mostly for their unwavering guidance all these months. To PhD students Marc and Julio who were also a part in helping me in several aspects of the project.

Next, to Misael, Jenny, Berta, Laia, "Piro", Mario, Julián, Rosa, Brij and Sina for all the conversations and stories shared during these months.

Last, but not least, to Sara for encouraging me to keep on, and especially, my parents who made all of this possible by investing continuously in my education.

Table of contents

Table of figures

1. Introduction

1.1. Mining, society and environment

1.1.1. Background

The extraction and processing of minerals is a prerequisite for the lifestyle of all advanced societies (Younger et al., 2002). The importance of the sulphide deposits of southern Spain and Portugal has been noticeable since the 4th century, when approximately 25 million tons of sulphide ore were mined from the region. These deposits, also known as the Iberian pyrite belt, typically contain 50% sulphur, 42% iron and between 2-8% of copper, lead and zinc (Van Geen et al., 1999).

Mining activity has left a widespread Cu and Zn contamination of sediments and organisms in the region. For instance, waters draining the region are highly acidic with high contents of Cd, Zn and Cu (España et al., 2005). A major concern around mining environmental impact was forged after the collapse of the retaining dam of a tailing reservoir in the region, on April 25 of 1998, resulting in the spill of 5 cubic hectometres of acid sludge, containing important quantities of heavy metals (Achterberg et al., 1999).

1.1.2. Sources of mine water contaminants

The minerals that represent economically valued ores are chemically stable under geological conditions. However, when excavated and exposed to atmospheric conditions, these minerals become unstable. Sulphur containing ores spontaneously dissolve when in contact with water, resulting in the release of metal ions from minerals such as sphalerite ($ZnS_{(s)}$), galena ($PbS_{(s)}$) or pyrite ($FeS_{2(s)}$) among others, in a process often called as “weathering” (Younger et al., 2002).

Weathering can be modelled as a series of redox reactions occurring when sulphide minerals dissolve in the presence of dissolved oxygen, as seen in equation (1). Thus, acidity and soluble metal ions are produced because of electron transfer to dissolved oxygen from sulphur and iron in the mineral phases, transforming them into their soluble forms (Akcil and Koldas, 2006).

$$MS\ (s)\ +\ 2\ O_2\ (aq)\ \rightarrow\ M^{2+}\ +\ SO_4^{2-} \qquad (1)$$

Where M is the metal atom present in the sulfide mineral (commonly Fe, Zn, Cu, Pb, Cd, Ni). In the case of Fe as metal atom, the weathering of $FeS_{2(s)}$ is represented by equation (2), in which acidity is represented by production of protons.

$$2\,FeS_2\,(s)\,+\,7\,O_2\,(aq)\,+\,2\,H_2O\,\rightarrow\,2\,Fe^{2+}\,+\,4\,SO_4^{2-}+\,4\,H^+ \quad (2)$$

When enough dissolved oxygen is present, the ferrous iron (Fe^{2+}) will be oxidized to ferric iron (Fe^{3+}), as shown in equation (3), consuming protons in the process.

$$2\,Fe^{2+}\,+\,\frac{1}{2}\,O_2\,+\,2\,H^+\rightarrow\,2\,Fe^{3+}\,+H_2O \quad (3)$$

However, acidity is heavily influenced because of Fe(III) reacting further to precipitate as iron hydroxide as in equation (4). Mine waters often achieve solubility equilibrium due to forward and reverse reactions being relatively rapid compared to the residence times of discharge water in mine workings.

$$2\,Fe^{3+}\,+\,6\,H_2O\,\leftrightarrows\,2\,Fe(OH)_3\,(s)\,+\,6\,H^+ \quad (4)$$

Consequently, mine water will accumulate solutes as minerals dissolve from these weathering reactions. Additionally, the pH will drop as protons are released to solution. This is a critical aspect of assessing mine water contamination since the solubility of metal ions is strongly pH dependent. Metal ions generally present increasing solubility with decreasing pH (Mcbride, 1989).

1.2. Treatment of polluted mine waters

The following section aims to establish a quick reference background on the different methods that have been studied in reference to the treatment of acidic mine waters. Environmental and economic concerns over the last decades have opened the door to the research and application of several techniques to improve the removal of contaminating ions in mine waters, as well as to explore methods to recover interesting ions from mining activity wastewaters in an approach to circular economy.

1.2.1. Conventional method

Conventional ODAS method (*o*xidation (O), *d*osing with *a*lkali (DA) and *s*edimentation (S)) is the predominant process in the mining industry. The main strategy of this method is to precipitate soluble ions into less soluble forms. As Fe(II) is present a pre-oxidation stage is needed. Then raise the pH through alkali dosing to force the precipitation of species containing the pollutant ions, and finally, the separation of the sludge from the rest of the water current (Younger et al., 2002).

It is important to note that the three steps (O, DA and S) do not always follow this strict order. In fact, the sequence of three processes is usually varied according to the particular situation.

For example, alkali dosing could precede oxidation to raise pH first to increase reaction rate of oxidation step.

1.2.2. Ion Exchange

Ion exchange is a reversible adsorption phenomenon driven by electrostatic interactions between an immobile phase, commonly referred to as the ion exchanger, and a liquid surrounding the immobile phase (Richardson et al., 2002). The exchanger contains ions held onto opposite charge functional groups on the surface of the exchanger matrix. As the liquid phase contacts the ion exchanger, ions held initially are released to the solution, while solvated ions present in solution are extracted by the charged functional groups.

Depending on the charge of the exchanging ions, the ion exchanger is termed either cationic or anionic, if the ions are positively or negatively charged respectively. Then, the exchange mechanism can be modelled by reaction (5) for cationic and (6) for anionic exchange:

$$R^-A^+ + B^+ \leftrightarrows R^-B^+ + A^+ \quad (5)$$

$$R^+A^- + B^- \leftrightarrows R^+B^- + A^- \quad (6)$$

In equations (5) and (6), R represents the functional groups on the surface of the exchanger, A represents the exchangeable ions, and B represents the target ion in solution. Often, the pair A-B are referred to as counter-ions in the literature (Inglezakis and Poulopoulos, 2006).

Taking into account that electroneutrality must be preserved in both phases; the exchange is regulated by equivalent numbers of charge. For example, a divalent ion would occupy two monovalent functional groups in exchange of two monovalent ions released to the solution from the exchanger (Inui et al., 2013).

The reversibility of the process allows the extraction of the extracted ions (named elution step) using a higher affinity ion containing solution to displace target ions from the resin. After this step, another solution must be put in contact to restore the original functionality of the resin (named regeneration step) (SenGupta, 2004).

1.2.2.1. Ion exchange resins

Currently, the basic form of an ion exchanger is a cross-linked polymer matrix, also known as resin, which has been functionalised by the attachment of an ionisable group. This has overcame stability issues of alumina-silicates as exchangers in presence of mineral acids, allowing, thus, exchanges involving hydrogen atoms (Richardson et al., 2002).

Due to the variety of chemical reactions available for functionalising polymers, several classes of resin can be defined (Cossio et al., 2012).

1.2.2.1.1 Strong and weak acid exchange resins

Strong acid exchange resins are named because of their chemical behaviour is similar of a strong acid. The functional groups present an acid form, where the exchangeable ion is H^+, and a salt form, where is a metal atom instead, usually Na^+. As these forms are highly dissociated, the exchange capacity is independent of solution pH. Regeneration to the hydrogen form is achieved by contact with a strong acid solution (HCl, H_2SO_4), while the salt form can be restored with a metal containing solution such as NaCl (Cossio et al., 2012).

On the other hand, weak acid exchange resins exhibit higher affinity for hydrogen ions than strong acid resins. Consequently, less acid for regeneration is required than for regenerating strong acid resins. However, resin capacity depends in part on solution pH due to its influence on the dissociation degree (Luqman, 2013).

1.2.2.1.2 Strong and weak base exchange resins

These resins follow an analogue approach than acid exchange resins. The main difference is that now the exchangeable anion is the OH^- group.

1.2.2.1.3 Chelating resins

Chelating resins are a group of materials with exposed complexing (chelating) groups, such as iminodiacetic acid, amino methyl phosphonic acid and bis-picolylamine among others, so that ion removal is based on the formation of complexes with metal ions only in certain pH ranges. Therefore, the selectivity of the separation is enhanced by ligands that possess high selectivity to the targeted metal ion (Garg et al., 1999).

1.2.2.1.4 Solvent impregnated resins (SIRs)

Solvent impregnated resins result from the necessity of a selective sorption at a lower cost than chelating resins, as the synthesis of chelating resins is complex and time consuming (Alexandratos and Ripperger, 1998). SIRs consist in a polymeric matrix impregnated with an available liquid ionic extractant. Therefore, SIRs combine the advantages of ion exchange for processing dilute solutions, with great mass transfer rates and selectivity factors of the extractants (Kabay et al., 2010).

1.2.2.2. Ion exchange operation

Fixed-bed ion exchange and continuous ion exchange are the two main technologies considered when treating solution streams (Denning and Dvorak, 2009). Both technologies are based on the packing of resin inside columns. Then, the solution stream is fed until resin regeneration has to be done.

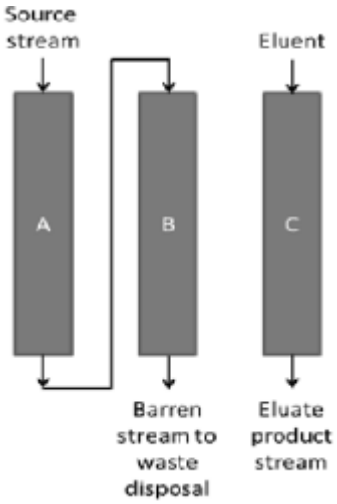

Figure 1 Lead-lag configuration for fixed-bed ion Exchange (Taute Thesis 2013) A: Lead column; B: Lag column; C: regenerating column

The fixed-bed ion exchange generally uses a three-column configuration, known as the lead-lag configuration, shown in Figure 1. The solution to be treated is fed to the first column (the lead column, A) and the outlet is fed to the second column (the lag column, B). Target ion will be extracted as solution saturates the lead column, while lag column collects any residual metal that exits lead column.

Once the exchange capacity in the lead column has been depleted, the solution stream is then fed to the lag column, which now becomes the lead column, and a freshly regenerated column acts now as the lag column. Former lead column is then regenerated (column C) so that there are always two columns on loading and one on elution (Inglezakis and Poulopoulos, 2006).

Following a similar approach, continuous ion exchange consists in a set of several smaller columns working simultaneously. Columns are fixed to a rotating base and feed solutions and regeneration solutions are fed continuously to the system, as in Figure 2 (Crittenden et al., 2012).

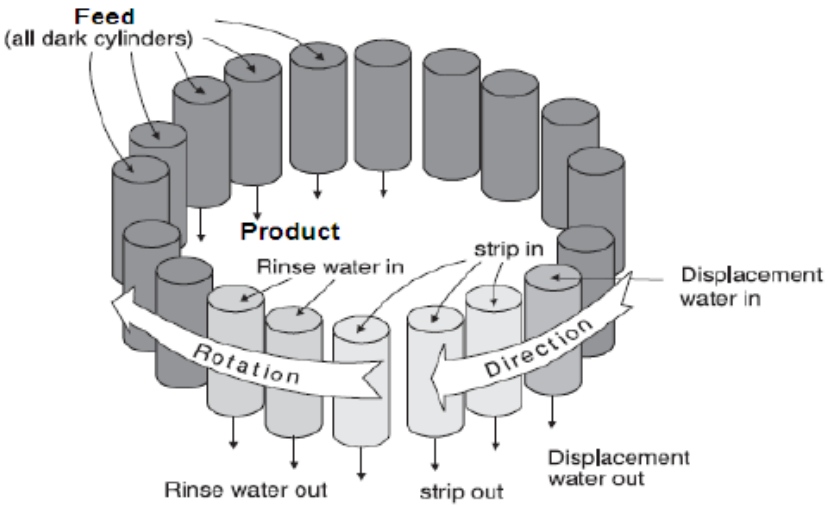

Figure 2 Continuous ion exchange configuration (Taute Thesis 2013)

Therefore, the columns rotate as the saturation is reached, so that there are always freshly regenerated columns on loading. Continuous ion exchange allows a reduced resin inventory, as well as reduced consumption of eluate and regeneration chemicals at the expense of higher maintenance costs (Crittenden et al., 2012).

1.2.2.3. Column breakthrough theory

When operating in column configuration, the solution to be treated flows through a packed bed of resin, until a determined concentration of the target ion is reached at the effluent. At this point, the resin is regenerated, usually by means of an acidic solution, for cation exchange resin thus eluting target metal ions from the resin.

When monitoring the adsorption process, it is common to generate breakthrough curves, obtained by measuring the metal concentration at the output stream. To do so, the solution is fed at a constant rate. Breakthrough curves are sigmoidal curves, similar to the one in Figure 3.

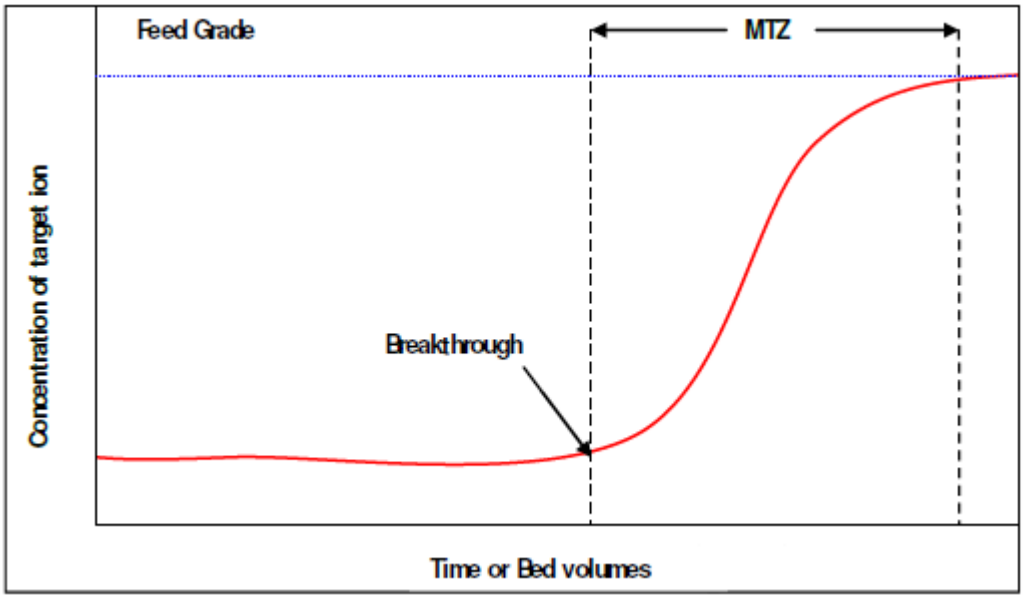

Figure 3 Generic breakthrough curve (Taute Thesis 2013)

The shape of the breakthrough curve can be explained as follows: when the stream enters the column, target ions are extracted by fresh resin, therefore extraction capacity is maximum at this moment. As solution keeps passing, the resin bed starts saturating. This phenomenon is reflected by the sigmoidal increase, also known as the Mass Transfer Zone (MTZ) (Inglezakis and Poulopoulos, 2006). The mass transfer zone moves through the column in a similar approach to the scheme in Figure 4.

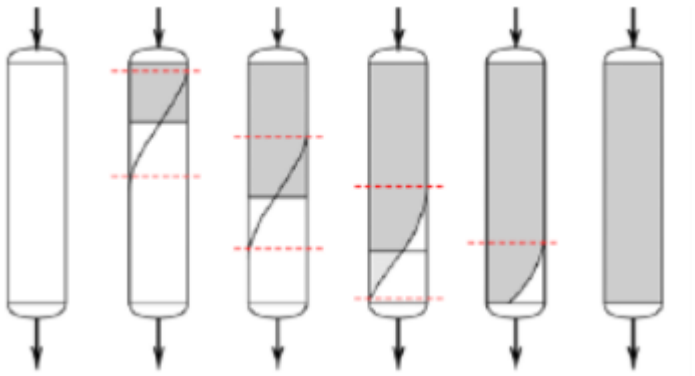

Figure 4 Mass Transfer Zone movement through the column. White section represents unused resin. Grey section represents exhausted resin

When the adsorption zone has moved through the column, the concentration of the adsorbate at the exit becomes equal to the feed concentration due to the exhaustion of the resin bed.

The breakthrough point is defined as the point where the output effluent reaches a target concentration. This point determines the maximum admitted loss of capacity, therefore, operation is stopped here and the column is regenerated.

Parameters such as capacity of the column with respect to the feed concentration, inlet flow rates and column diameter and height, among others, influence the characteristic shape of the curve (Ghorai and Pant, 2005). For example, the influence of the flow rate is shown in Figure 5.

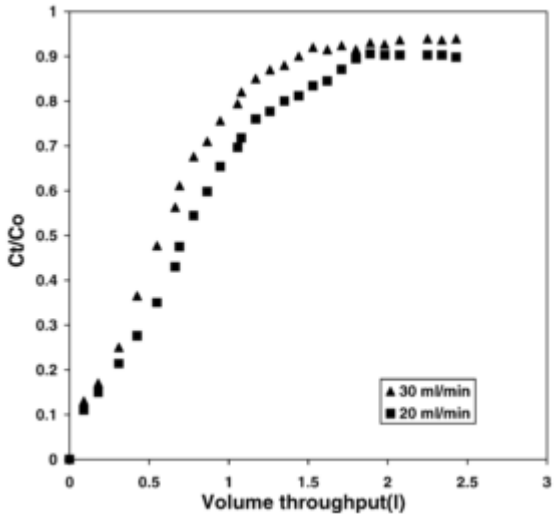

Figure 5 Breakthrough curves for different flow rates (Ghorai and Pant, 2005)

When increasing the inlet flow rate, the time to reach the breakthrough point decreases, and the curve becomes steeper as a consequence of the residence time not being long enough for adsorption equilibrium to be reached (Ghorai and Pant, 2005).

1.2.2.4. Ion exchange for Zinc and Copper separation

Ion exchange is commonly used in several industries, such as water purification, food, for example in the decaffeination of coffee, tea and cocoa (Kammerer et al., 2011), and catalysis, as in the oxidation of organic compounds (Shaabani et al., 2003), among others. In hydrometallurgy it plays an increasingly important role in the recovery of base metals (such as Pb, Cu and Zn) from mine waters (Barton, 1978).

Simpson and Laurie, (1999) tested the selectivity of several resins for zinc removal in Zn rich waste liquors (480 g/L) containing Pb (1000 mg/L) and Cu (300 mg/L) as majoritarian competitors. Results of the study determined that Lewatit VP OC 1026 (D_2EHPA impregnated resin) showed the greatest selectivity for zinc removal. Other tested resins, such as Lewatit TP 207 and Purolite S930 (both chelating resins), showed greater selectivity to Pb, Cd and Cu.

Furthermore, Taute (2013) observed no selectivity between Fe and Zn when working with Lewatit VP OC 1026 at a pH below 2.5 in solutions containing iron, due to the rapid oxidation of Fe(II) to Fe(III), which was in concordance to the selectivity data available from Lanxess (Lanxess, 2011a).

In addition, Taute, Sole, and Hardwick (2013) observed that only 10% to 15% Fe was removed from the resin when eluting with 100 g/L H_2SO_4. In consequence, resin capacity would eventually decrease due to the accumulation of Fe(III). Keeping Fe ion levels below 50 mg/L and pH between 2.5 and 2.9 proved to be the best conditions for Lewatit VP OC 1026 to minimise resin fouling. Stronger regenerants such as HCl can be used to remove Fe from the resin, as Ma et al. (2015) reported 70% Fe(III) removal from an aqueous D_2EHPA solution with 110 g/Lto 180 g/L M HCl.

Rudnicki, Hubicki, and Kołodyńska (2014) used Lewatit TP 207 (iminodiacetic resin), in its sodium form, for processing waste streams containing Cu(II), Zn(II) and Ni(II) adjusting the solution to different pH. Batch experiments determined that adsorption equilibrium was achieved within an hour. Moreover, batch results showed 90% Cu extraction in the pH range from 1 to 7, while Zn and Ni extraction were below the 20% for pH < 3.

Valverde et al. (2004) also studied Lewatit TP 207 selectivity towards Cu, Zn and Cd in batch experiments under vigorous stirring for 24 h. Equilibrium data at 25ºC and pH ranging from 4 to 7 proved higher selectivity for Cu towards Zn and Cd following a Langmuir-type model.

1.3. Recovery of metal ions by electrorecovery technologies (Electrowinning)

1.3.1. Overview

Once the metal extraction and concentration process has been completed, electrochemical techniques can be applied to produce or recover the metals from the concentrated solutions. Figure 6 schematically shows the steps between hydrometallurgy process and the reduced metal obtainment.

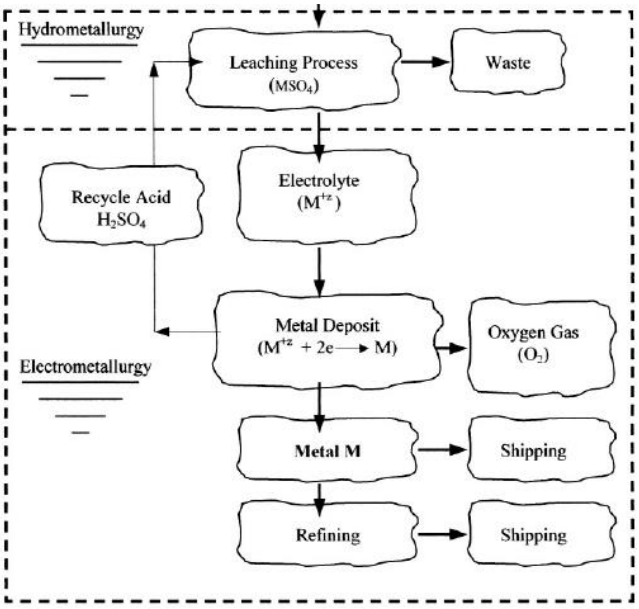

Figure 6 Block diagram for electrowinning of a metal M (Perez, 2004)

Hydrometallurgical processes include techniques such as solvent extraction and ion exchange for extracting metals from ores, resulting in a solution containing the desired metal cations and impurities. Metal recovery then is carried out by electrolysis of the obtained solution, which is used as the electrolyte. During electrolysis, the following reactions take place (Perez, 2004):

(Anode) $$2\,H_2O \rightarrow 4\,H^+ + O_2(g) + 4\,e^- \quad (7)$$

(Cathode) $$2\,M^{2+} + 4\,e^- \rightarrow 2\,M(s) \quad (8)$$

(Overall) $$2\,M^{2+} + 2\,H_2O \rightarrow 2\,M(s) + 4\,H^+ + O_2(g) \quad (9)$$

From the anodic reaction (7), it can be concluded that water molecules decompose to produce both proton and hydroxyl ions. On the other hand, the cathodic reaction (8) will take place for all cationic impurities present in the solution. In electrowinning, the reduced metal generated from the cathodic reaction, is recovered as a deposited layer on the electrode surface. Refining consists in dissolving the obtained solids in a fresh acidic solution, and depositing the metals again on new cathodes to increase purity (Perez, 2004).

Electrowinning takes places in electrolytic cells containing several sets of anodes an cathodes, connected in parallel, to reduce potential drops and increase the available surface for metal deposition (Perez, 2004). A typical scheme is shown in Figure 7.

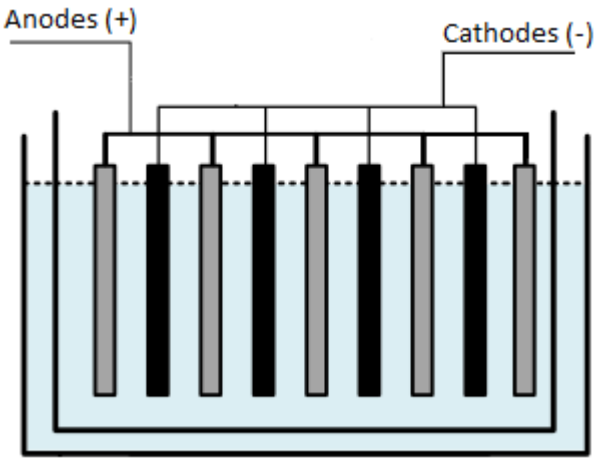

Figure 7 Electrowinning cell (modified from (Kartikaningsih et al., 2016)*)*

Cathodes are connected to the negative pole of the power supply in order to attract the metallic cations. As the deposition takes place in all the surface of the cathodes, the number of anodes required is the same as the number of cathodes plus one, to ensure proper current distribution.

Once enough deposition has occurred, the metal layer is mechanically removed due to the low interactions existing between the deposit and the substrate (Perez, 2004).

1.3.2. Factors influencing metal deposition

The main factors controlling electrolytic processes are current and electrode potential (Gamburg and Zangari, 2011).

Faraday's law of electrolysis establishes the relationship between the metal mass and the charge needed for the deposition of the metal. At constant current, Faraday's law can be expressed as a function of intensity and time, as follows in equation (10) (Zoski, 2007).

$$m = \frac{I * t * M_w}{z * F} \qquad (10)$$

Where m is the deposited mass (g), I is the current intensity (A), t is the time (s), M_w is the atomic weight of the metal (g/mol), z is the electronic valence and F is the Faraday constant (A·s/mol). Faraday's law is used to calculate the amount of metal deposited during electrolysis or to determine the time to achieve a determined deposited mass.

The potential of the electrode is the potential drop between the solution and the bulk of the metal. As this potential cannot be measured experimentally, it is conventional to measure the electrode potential with reference to standard reference electrodes, such as calomel or silver chlorides electrodes (Gamburg and Zangari, 2011). For metal deposition to occur, the applied

potential must be greater than the sum of the anode and cathode standard potentials (Perez, 2004).

Other factors such as solution temperature, pH and substrate may influence the electrodeposition process (Gamburg and Zangari, 2011).

Operation temperature is usually in the range from 15 to 70 ºC. Elevated temperatures improve electric conductivity and solubility of the metal species. However, electrolyte evaporation and and corrosion processes are accelerated (Gamburg and Zangari, 2011).

Acidity of the electrolytic solution has to be stable and constant through the entire cell volume, especially near the electrode, as hydrogen generation during the electrolysis leads to higher pH, resulting eventually in metal hydroxide precipitation. This can be accomplished by buffering the electrolyte and by proper agitation (Gamburg and Zangari, 2011).

In addition, hydrogen bubbles limited diffusion effects, current efficiency and incremented the porosity of the deposited metal layer (Nikolic and Popov, 2010).

Moreover, the use of additives on the electrolyte is a widespread practice (Gamburg and Zangari, 2011). For example, several compounds such as glue, sodium lignin sulphonate, and gelatine have been added to the electrolyte, to improve Zn electrowinning increasing the current efficiency of the cell (from 50% to 60%) for lower concentrations of 10 mg/L of additive. (Venkateswaran et al., 1996).

Traditionally, insoluble metal anodes for Zn electrodeposition are mainly made of Pb or Pb-Ag alloys, while Pb-Sb alloys are used in Cu electrowinning (Moskalyk et al., 1999). Cathode sheets are usualy made out of metal M, stainless steel or Ti (Perez, 2004).

1.4. Objectives

1.4.1. Project scope

The present project aims to establish a process for Zn and Cu separation in Zn rich and Cu rich streams respectively from mine water effluents by means of fixed-bed ion exchange columns. Studies on real water will be carried out to select the optimal ion exchange resins for maximum Zn and Cu selectivity. Subsequently, metal recovery from the enriched streams will be evaluated by means of electrochemical methods.

On the other hand, the optimization of the operation conditions and the scaling-up of the stages are beyond the scope of this project.

1.4.2. Specific Objectives

- Evaluate the optimal pre-treatment to reduce the presence of Al and Fe from the acid mine waters.
- Evaluate ion-exchange resins for selective Zn and Cu extraction in batch mode.
- Determine the optimal pH window for Zn and Cu extraction in batch system.
- Evaluate adsorption, elution and concentration capability for Zn and Cu separation from real mine waters through ion exchange experiments in column mode, determining concentration factors and separation percentages for both ions.
- Determine the operation conditions such as cycle times, ion elution and resin regeneration in column system.
- Evaluate the conditions for Zn and Cu recovery in metal form by means of electrowinning process.
- Determine the feasibility of electrochemical methods for Cu and Zn recovery.

2. Experimental Procedure

2.1. Process overview

This project is originated from the need to valorise acidic mine water streams generated during mining operation. As mentioned above, acidic mine streams are often a source of valuable metals such as Zn and Cu. Environmental concerns and the increasing demand for raw materials have arisen the need of assessing the value of acidic mine streams as well as to seek processes for the recovery of the valuable metals. Consequently, the concept of this project for the extraction and recovery of valuable metals from acidic mine streams is shown in Figure 8.

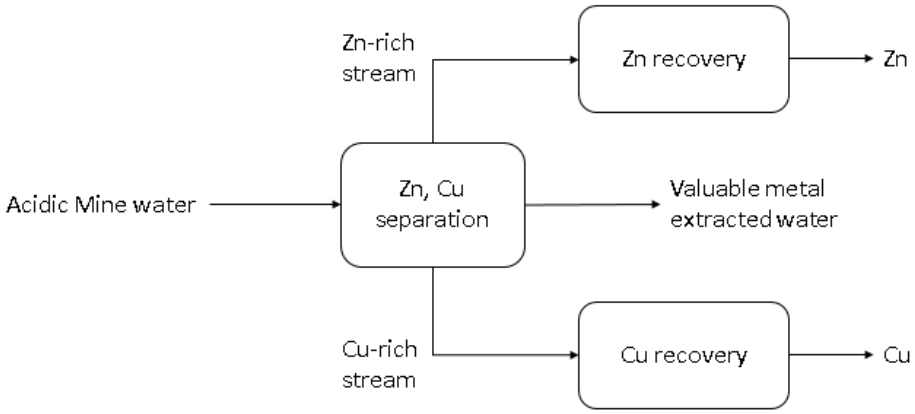

Figure 8 Scheme of the processes to separate and recover valuable metals

In order to recover both Zn and Cu, a highly selective operation is required. From the analysis of the current literature, it was decided to perform the separation by means of ion exchange, while the metal recovery is intended to be in metal form. Thus, electrowinning is selected as process to reduce the dissolved Zn and Cu ions in the last stage.

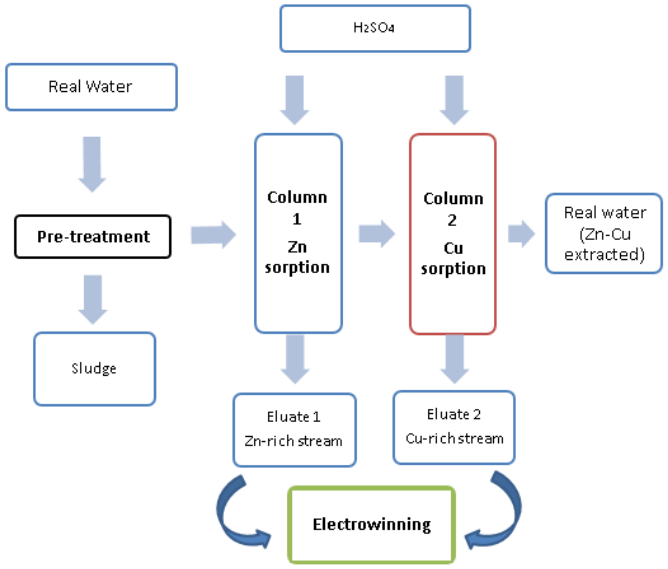

Figure 9 Experimental process flow sheet for the Cu and Zn recovery process

In consequence, Figure 9 contains the updated desired flow sheet to test during the experimental process. Following this approach, the ion exchange stage was carried out in two columns to generate two streams concentrated in Zn and Cu respectively. The first column contained a Zn selective resin and was fed with the real mine water. The second column contained a Cu selective resin and was fed with the stream resulting from the first column (free of Zn).

For both columns, following resin bed saturation, a solution of sulphuric acid was pumped, releasing the extracted ions. Thus, a Zn rich stream was generated from the first column, and a Cu rich stream was generated from the second. Then, both streams are treated individually in an electrowinning step to recover Zn and Cu.

Previous ion exchange stage, a pre-treatment step is planned to remove solids and precipitates to prevent column clogging.

2.2. Characterization of acidic mine water samples

A total volume of 100 L from a real mine water, from south-west Spain, was available to perform the experiments planned in this project. Information about the composition provided by the sample supplier is shown in Table 1.

Concentrations in mg/L

Ca	Mg	Cu	Zn	Fe	Mn	Na	Al	S
550	2000	300	850	160	200	100	400	4950

Table 1 Estimated water composition

In order to verify the data supplied, sample composition was analysed by Inductively Coupled Plasma Mass Spectrometry (ICP-MS) and Inductively Coupled Plasma Optical Emission Spectroscopy (ICP-OES). The pH of the sample was measured using a Crison GLP 22 pH meter. Fe concentration reflects the total concentration accounting for Fe(II) and Fe(III). According to the previous experience in acid mine waters, it was expected than most of the Fe present in solution is in the form of Fe(II).

2.3. Pre-treatment for Fe(II) and Al(III) removal

Fe and Al were removed from the samples in a three-stage process following an ODAS approach. In the first stage, 1 ml of H_2O_2 35% (v/v) per litre of acid mine water was added to oxidize Fe (II) to Fe (III). Peroxide volume dosed was calculated as twice the amount of Fe present per litre of water.

Then in a second stage, Fe and Al were precipitated as hydroxide and hydro-sulphate precipitates by increasing the pH to 3.7-3.8 for Fe, and to 4.6-4.8 for Al with NaOH 2M. Lastly, precipitates and suspended solids were removed by gravity filtration using a filter paper. Figure 10 resumes the process previously explained.

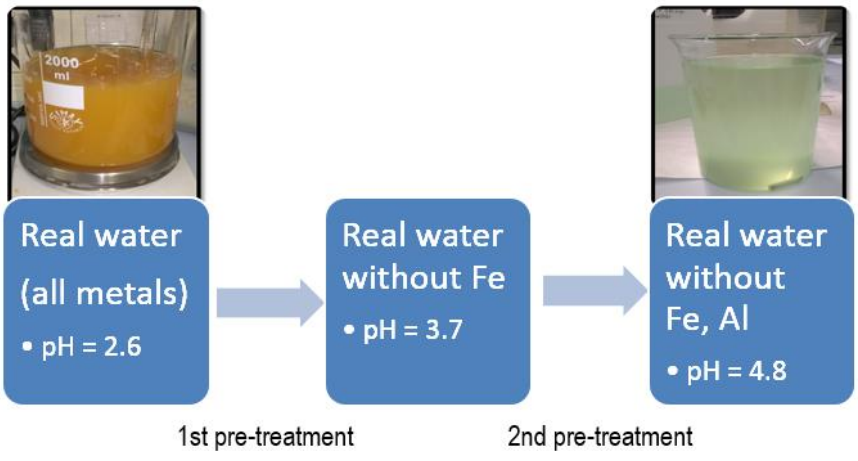

Figure 10 Fe and Al elimination pretreatment process

Solids were dried and grinded for analysis by Field Emission Scanning Electron Microscopy (FESEM), and liquid samples after each pre-treatment step were analysed by ICP-OES and ICP-MS to determine the efficiency of the pre-treatment step.

2.4. Ion exchange resins for Zn and Cu separation and concentration

Based on the information reviewed in section 1.2.2.1, two SIRs: Lewatit VP OC 1026 (Figure 11 *a)*) and Lewatit TP 272 (Figure 11 *b)*); and a chelating resin: Lewatit TP 207 (Figure 11 *c)*) were selected to perform batch adsorption experiments.

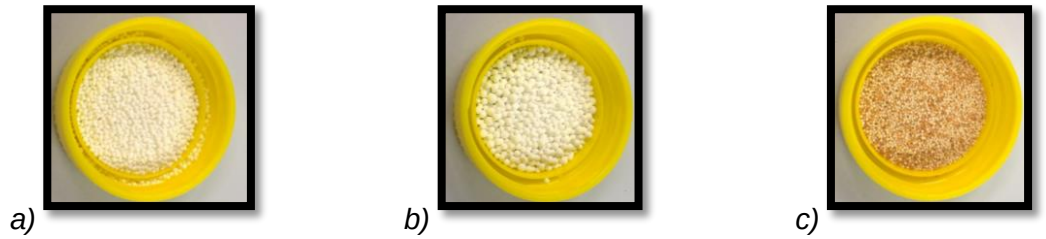

a) *b)* *c)*

Figure 11 Aspect of the resins used in this study: a) Lewatit VP OC 1026 b) Lewatit TP 272 c) Lewatit TP 207

A brief summary of the properties of each resin is presented in Table 2.

RESIN	LEWATIT VP OC 1026	LEWATIT TP 272	LEWATIT TP 207
FUNCTIONAL GROUP	D_2EHPA	Bis-(2,4,4-trimethylpentyl) phosphinic acid	Iminodiacetic acid
IONIC FORM	H^+	H^+	Na^+
DENSITY (g/mL)	0,97	0,97	1,17
CAPACITY	13 g Zn/L	12,5 g Zn/L	2,2 eq H/L
SELECTIVITY	Ti>Fe(III)>In>Sn>Sb>Bi>Vo>Be>Al>Zn>Pb>Cd>Ca>Mn>Cu>Fe(II)>Co>Ni>Mg>Cr>>>Alkali	Fe(III)>Zn>Al>Cu>Co>Mg>Ca>Ni	Cu>VO>UO>PB>Ni>Zn>Cd>Fe(II)>Be>Mn>Ca>Mg>Sr>Ba>>>Na
REGENERATION	Strong acid (HCl, H_2SO_4)		
CONDITIONING	Not required	Not required	NaOH
SOURCE	(Lanxess, 2011a)	(Lanxess, 2011b)	(Lanxess, 2011c)

Table 2 Resin properties obtained from resins data-sheets

Resins VP OC 1026 and TP 272 are impregnated with a compound containing the extracting agent (D_2EHPA or Bis-(2,4,4-trimethylpentyl) phosphinic acid respectively) . Therefore, both resins can be used directly. On the other hand, resin TP 207 may contain groups with both, neither or only one of the functionalities in Na^+. For that reason, the resin is conditioned with NaOH 1M prior to its use to ensure that all functionalities are in the same ionic form. In addition, NaOH conditioning must be done before every exhaustion cycle for heavy metal extraction (Lanxess, 2011c). Resins VP OC 1026 and TP 272 must not be exposed to strong bases to avoid the loss of the active ingredient.

2.5. Batch experiments for resin evaluation

The following experiments were designed to evaluate resins selectivity towards Zn and Cu as a function of pH. Three types of streams were prepared to study the performance of the selected resins:

1. Real water: corresponds to the original water sample available, without applying any pre-treatment.
2. Real water without Fe: corresponds the water resulting from the elimination of Fe(III).
3. Real water without Fe and Al: corresponds the water resulting from the elimination of Fe (III) and Al (III).

The batch experiments were carried out with 20 mL of aqueous solutions and 5 g (for TP 272 and VP OC 1026) or 1.88 g of resin (TP 207) and were added in glass tubes for each aqueous solution sample, resin and pH combination. The pH range studied was1; 1.5; 2; 2.5; 3; 4 and 5, for real water and real water without Fe and Al, and pH 1; 2; 3 for real water without Fe. Mass was selected so the same amount of exchange equivalents were available for the sorption and in excess in relation to the ions in solution.

Later, glass tubes were equilibrated by agitation for 2 hours at room temperature (25ºC). Every 30 minutes, sample pH was measured and 1 mL fraction was collected in Eppendorf tubes. Then, pH was adjusted back to the initial value and the glass tubes were agitated. The fractions corresponding to 2 hours of experiment were analyzed by ICP-MS and ICP-OES. Duplicate experiments are performed to increase the accuracy of the results.

2.6. Column experiments

Column experiments were performed to assess the resins sorption capacities for Zn and Cu in a continuous system by using breakthrough curves. Moreover, after the evaluation of optimal conditions for adsorbed metal separation, the elution profiles were obtained.

Figure 12 a) Zn column b) Cu column

Following the scheme presented in Figure 9, the first separation stage was focused for Zn adsorption. 30 g of resin were packed in a 2.5 cm internal diameter column and 13 cm height, as can be seen in Figure 12 *a).* The remaining volume was filled with glass wool; hence, the length of the resin bed was 11 cm.

For Cu separation, 1.1 cm internal diameter column and 7.5 cm height was loaded with 4 g of resin, while the remaining volume was filled with glass

wool, as displayed in Figure 12 *b)* Therefore, the length of the resin bed is 5 cm after packing the column.

2.6.1. Bed Volume and porosity determination

Prior to starting adsorption experiments it is important to define a key parameter in column operation. The bed volume (BV) can be defined as the free volume in a packed bed column (Crittenden et al., 2012). Bed volume is described by equation (11).

$$BV = \frac{Q * t}{V_b} \quad (11)$$

Where *BV* is the bed volume, *Q* is the flow rate (mL/min), *t* is the elapsed time (min) and V_b is the volume of the reactive bed.

Notice that BV is a non-dimensional magnitude; therefore its importance in the existing literature, as BV allows relating breakthrough curves to different columns, as the definition must be preserved since it mainly depends on the column dimensions. Consequently, it is a key magnitude when scaling up or down systems.

The volume of the reactive bed is defined in equation (12):

$$V_b = \pi * r^2 * h_b * \varepsilon \quad (12)$$

Where *r* is the internal radium of the column (cm), h_b is the length of the resin bed (cm) and ε is the porosity.

Experimentally, the porosity can be determined measuring the conductivity of a NaCl solution passing through the column. The conductivity profile should follow a sigmoidal tendency, as shown in Figure 13 (Shackelford et al., 1999).

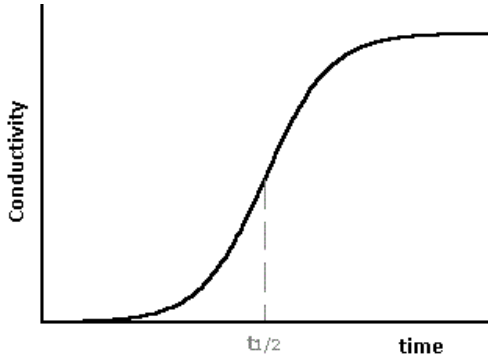

Figure 13 Conductivity profile obtained after porosity test

Therefore, the porosity can be calculated as the ratio between the NaCl solution volume that has passed through the column at the inflection point ($t_{1/2}$ in Figure 13) and the total volume of the column, as it is reflected in equation (13) (Crittenden et al., 2012).

$$\varepsilon = \frac{Q * t_{1/2}}{V_{column}} \quad (13)$$

Where Q is the flow rate (mL/min), $t_{1/2}$ the inflection point (min) and V_{column} is the total column volume (mL).

For both Zn and Cu columns, a 0.05 M NaCl solution was used. The flow rate for Zn column was set to 0.5 mL/min, whereas for Cu column was 0.25 mL/min. Conductivity was measured using a Crison GLP 31 conductivity meter. Experiments were performed by duplicate to increase the accuracy of the results.

2.6.2. Metal adsorption experiments

Column experiments were carried out to mainly determine the breakthrough curves for Zn and Cu. The experimental set up for both columns was the same and it is presented in Figure 14.

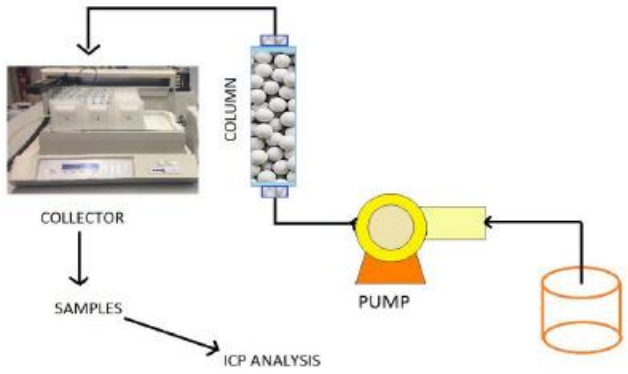

Figure 14 Column process schematic. Modified from (Manzano, 2017)

Solutions were fed to the column by means of a peristaltic pump. Flow direction in the column is always bottom to head to ensure that the column is flooded, therefore, all the empty volume is occupied, and the liquid is full contact with the resin bed.

Firstly, a preliminary column test for metal adsorptions was carried out at 6 BV/h (equivalent to 2.6 mL/min for Zn column and 0.34 mL/min for Cu column) to determine the time needed to reach complete saturation of the resin. The time for this preliminary study was about 60-70 h. Afterwards, flow rate was decreased to 5 BV/h (2 mL/min) to delay the breakthrough point, and increased for Cu to 24 BV/h (1.36 mL/min) to reduce the experiment duration around 24 h.

Six adsorption experiments in total were carried out for Zn: four full adsorption cycles (until complete saturation of the bed volume), and two until the breakpoint was reached. On the other hand, for Cu adsorption, three full adsorption cycles were studied.

The batch experiments determined the type of resin and pH that was used in column experiments.

Finally, fractions collected through the automatic sampler were analyzed by AAS to determine the evolution of the breakthrough curve, and by ICP-OES and ICP-MS to determine the concentrations in solution. In addition, pH and conductivity were measured for each sample.

The adsorbed metal mass was determined by integrating the area above the breakthrough curve for each ion. As C/C_0 represents the outlet concentration, a simple mass balance defines adsorbed concentration as $(1-C/C_0)$. Therefore, to obtain the adsorbed mass can be obtained from equation (14).

$$m_{ads} = C_0 \int_0^{V_{sat}} \left(1 - \frac{C}{C_0}\right) dV \qquad (14)$$

Where m_{ads} is the adsorbed metal mass (mg), C_0 is the feed concentration (mg/L) and V_{sat} is the total volume of solution that passed through the column at the saturation point.

Numerical integration by the trapezium rule was used to split the calculation into smaller areas, as shown in Figure 15, to solve equation (14).

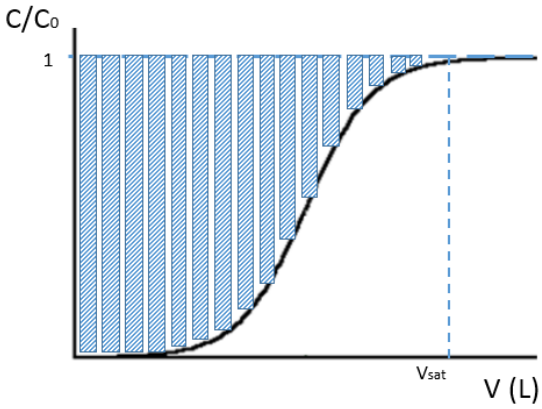

Figure 15 Graphical representation of the numeric integration

The trapezium is defined by equation (15).

$$\int_a^b f(x)\,dx \approx \sum_{k=1}^{N} \frac{f(x_{k-1}) + f(x_k)}{2} \Delta x_k \,. \qquad (15)$$

Where Δx_k, represents the width of each subarea (L) between the current integration point and the previous and $f(x_{k-1})$ and $f(x_k)$ are the value of $(1\text{-}C/C_0)$ for the previous and current integration points respectively, which are equivalent to the length of the two bases of the trapezium.

Resin capacity was calculated afterwards by equation (16)

$$Q = \frac{m_{ads}}{m_{res}} \tag{16}$$

Where Q is the resin capacity (mg metal/g resin), m_{ads} is the adsorbed mass for a determined metal (mg) and m_{res} is the resin mass in the column (g).

2.6.3. Metal elution experiments

After each exhaustion cycle was completed, the release of the extracted ions was performed to restore resin capacity. The elution was carried out with a 100 g/L H_2SO_4 at half flow rate of adsorption process. Samples were taken manually with higher frequency during the first minutes of elution in order to represent the elution peak and to determine the concentration factor reached in the sorption/desorption process. Samples were analyzed by AAS in order to stop the elution at the minimum possible volume. Conductivity and pH were also measured during the process. Metal concentration will be determined by ICP-OES and ICP-MS.

Once the elution was completed, due to the different nature of the selected resins different steps were taken:

For resin Lewatit VP OC 1026, metal extraction is described by equation (17).

$$2R_2PO_2H_{res} + Zn^{2+} \leftrightarrows R_2PO_2 - Zn + 2H^+ \tag{17}$$

When H_2SO_4 passed through the resin bed, the reaction was reverted. Hence, the resin extracted the protons and Zn was released to the solution. In consequence, the resin returned to its initial form, thus, Zn sorption could take place again. Therefore, the last step prior to the beginning of another adsorption cycle was rinsing the column with Milli-Q water to displace the remaining acid out of the system.

Zn column was rinsed at a flow rate of 1 mL/min around 18 h, when the pH of the effluent reached the initial pH measured on the adsorption cycle.

Nevertheless, for resin Lewatit TP 207 the process involved a variation.

$$2\,R - NHPOO^-Na^+ + Cu^{2+} \leftrightarrows (R - NHPOO^-)_2Cu^{2+} + 2\,Na^+ \tag{18}$$

As can be seen in equation (18), when Cu sorption took place, the initial sodium ions were released to the solution. When H_2SO_4 passed through the resin bed, the Cu ions were exchanged by protons, following the reaction described in equation (19).

$$(R-NHPOO^-)_2Cu^{2+} + 2\,H^+ \leftrightarrows 2\,R-NHPOO^-H^+ + Cu^{2+} \quad (19)$$

Therefore, the iminodiacetic groups now were found in the acidic form. To recover the initial sodium form, the resin bed was regenerated with a sodium containing solution.

The regenerate solution consisted of 1 M NaOH solution, and it was fed to the column at half the elution flow rate during 1 h 45 min. After that, the column was rinsed with Milli-Q water at the elution flow rate during an hour (slow cleaning), and then at 1 mL/min (quick cleaning) for 24 h.

The concentration of the eluted stream was obtained from the area of the elution profile peak, in a similar approach to the calculation of the adsorbed mass from the breakthrough curve, as shown in Figure 16.

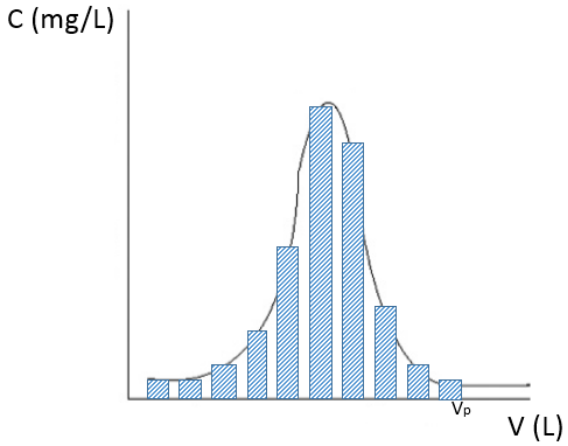

Figure 16 Elution peak numerical integration

The concentration for a given metal in the elution stream is therefore defined by equation (20)

$$C_{elu} = \int_0^{V_p} C\,dV \quad (20)$$

Where C is the measured metal concentration (mg/L), V_p, the volume of elutant required for the complete desorption of the metal ion (L) and C_{elu} the metal concentration in the elution stream (mg/L). Finally, the concentration factor of the separation stage was determined for each metal ion by equation (21).

$$FC = \frac{C_{elu}}{C_0} \quad (21)$$

Where C_{elu} is the metal concentration in the elution stream, and C_0 is the metal concentration in the feed solution for the adsorption process.

2.7. Preliminary study on electrowinning

A preliminary set of experiments was designed for studying the recovery of Zn^{2+} and Cu^{2+} ions, from elution streams, as metal form by electrochemical process.

Experiments were performed in a 3 L electrolytic cell. In the center of the cell, a 12x12 cm AISI 304 stainless steel cathode (Figure 17 *a)*) was disposed. A 10x10 cm iridium oxide coated Ti mesh anode (Figure 17 *b)*) was situated each side of the cathode with a separation of 2 cm from the central cathode.

An adjustable 40 V power supply was used as the current source. Metal deposition was carried out at constant current intensity.

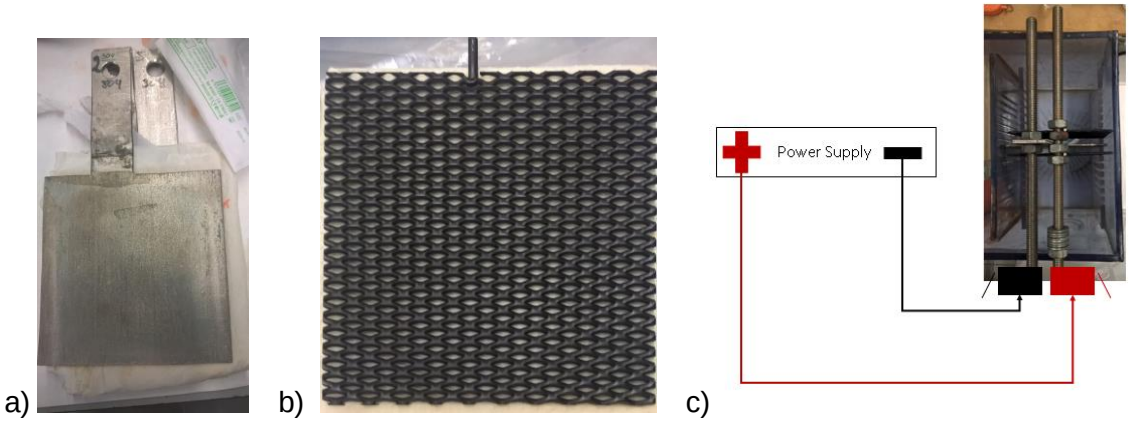

Figure 17 a) Electrolytic cell connection schematic b) Iridium oxide mesh anode c) AISI 304 steel cathode

The anodes were connected to the positive terminal of the power supply, and the cathode was connected to the negative (as shown in Figure 17 *c)*), thus cations are deposited on the steel surface. If the polarity was inverted, the steel plate would dissolve due to redox equilibrium. Another additional issue was the risk of short-circuit due to the small distance between the cell terminals, implying that applied current passed through the less resistive route, hence decreasing electrolysis performance significantly. Therefore, verifying the cell connections is required before turning on the power supply.

The theoretical deposited mass can be calculated by Faraday's law, which is described in equation (22):

$$m = \frac{I * t * M_w}{z * F} \qquad (22)$$

Where *m* is the deposited mass (g), *I* is the current intensity (A), *t* is the time (s), M_w is the atomic weight of the metal (g/mol), *z* is the valence and *F* is the Faraday constant (A·s/mol). In the experiments, the deposited mass will be determined by gravimetric analysis of the cathode. Therefore, current efficiency (ϵ) was calculated by Equation (23).

$$\epsilon = \frac{obtained\ mass\ (g)}{theoretical\ mass\ (g)} * 100 \qquad (23)$$

The applied current intensity was calculated by Faraday's Law (equation (16)) to deposit all Zn or Cu mass within an hour. For Cu deposition, the theoretical required intensity for complete extraction, based on the Cu concentration on the elution stream for 3 L of solution, was 1 A. Therefore experiments were performed at 0.5 A; 1 A and 2 A.

For Zn deposition, the theoretical deposition of all the Zn contained in solution, based on the concentration on the elution stream for 3 L of solution, occurred at 7 A, hence 4 A; 7 A and 10 A were applied. In addition, for Zn, the effect of pH on the deposition was studied at 7 A for pH 0 and pH 4.5.

Liquid samples for electrolytic cell were collected every 10 minutes to measure conductivity, pH, and Zn and Cu concentrations by AAS. Furthermore, recovered metals (solids) from cathode surface were analyzed by FSEM.

3. Results and discussion

3.1. Real water sample characterization

Results for the ICP analysis of the real water sample are shown in Table 3.

Concentrations in mg/L

Zn	Cu	Fe	Al	Cd	Mn	Mg	Na	Ca	S
747	280	109	363	2,4	196	1787	0	501	4237

Table 3 Mine water sample composition

The pH of the mine water sample was of 2.7±0.1.

3.2. Pre-treatment for removal of Fe (II) and Al (III)

The main purpose for this analysis was to determine the Fe and Al removal capability of the sample pre-treatment against the loss of Cu and Zn. However, it was also interesting to assess what happened to the rest of the metals during this stage. Removal % shown in Table 4 is always referred to the initial water sample at pH = 2.7.

	Removal %							
pH	**Zn**	**Cu**	**Fe**	**Al**	**Cd**	**Mn**	**Mg**	**Ca**
3.70	0	0	96	4	0	0	0	10
4.80	2	8	100	90	2	5	2	10

Table 4 Pretreatment metal removal evaluation

Increasing pH to 3.7 the 96 % of Fe was removed. Then, it can be concluded that the oxidation by means of H_2O_2 dosage was successful, since the vast majority of iron (96%) was eliminated at low pH. It can also be observed that a little amount of Al and Ca started to precipitate at this point. On the other hand, Zn losses at this stage were zero. Results at this stage were consistent with the work of Wei, Viadero, and Buzby (2005), which reported 98% Fe elimination and 2% Al elimination by precipitation at pH>3.5 after the oxidation of Fe(II) to Fe(III) in presence of oxygen.

Moreover, increasing the pH up to 4.8, all Fe was extracted from the solution (100%) and Al removal reached 90%. At the same time, results showed that all other metals started to precipitate whilst Zn and Cu did not excess 10% removal. The results of the second step can also be compared with the work of Wei, Viadero, and Buzby (2005) as they also reported 97%

Al removal at pH=5.0, as well as around 5-10% removal of Ca, Mg, Mn and Zn, and approximately 15% of Cu losses. Other authors, such as Matlock, Howerton, and Atwood (2002), achieved 100% Fe, Pb and Mn removal using BDET. However, the process took 20 h and the ligand showed great selectivity for Cu additionally.

In order to verify the results obtained measuring the concentration in the liquid phase, ICP analysis are contrasted with the Hydra and Medusa software database. In addition, solid samples were analyzed by FESEM.

a) b)

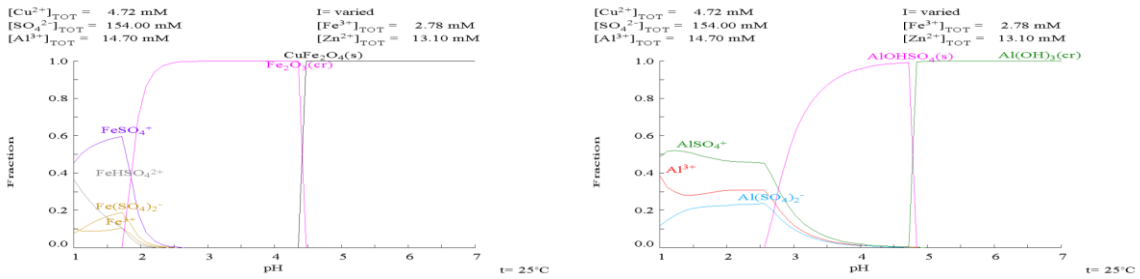

Figure 18 Hydra-Medusa fraction diagrams for Fe (a) and Al (b) respectively

The Hydra-Medusa curves for Fe (Figure 18 *a)*) and Al (Figure 18 *b)*) showed that insoluble compounds were predominant for Fe at pH > 2, and for Al at pH > 3. Therefore, precipitates containing both elements were expected at pH 3.7 and 4.8 respectively.

In order to perform a semi quantitative analysis of the precipitate, three different solid sections were analyzed.

Spectrum	In stats.	O	Mg	Al	Si	S	K	Ca	Fe	Total
Spectrum 1	Yes	47.48	0.48	1.66	1.00	7.02	0.26	1.38	40.72	100.00
Spectrum 2	Yes	49.89	0.56	1.92	1.15	7.75	0.25	1.58	36.90	100.00
Spectrum 3	Yes	48.43	0.51	1.82	1.36	7.53	0.38	1.12	38.85	100.00
Mean		48.60	0.52	1.80	1.17	7.43	0.30	1.36	38.82	100.00
Std. deviation		1.21	0.04	0.13	0.18	0.37	0.07	0.23	1.91	
Max.		49.89	0.56	1.92	1.36	7.75	0.38	1.58	40.72	
Min.		47.48	0.48	1.66	1.00	7.02	0.25	1.12	36.90	

a)

Spectrum	In stats.	O	F	Na	Mg	Al	Si	S	Ca	Mn	Cu	Zn	Total
Spectrum 1	Yes	62.62		0.77	2.01	15.42	0.77	12.20	1.86	0.80	2.20	1.36	100.00
Spectrum 2	Yes	61.66	1.34	0.98	2.01	14.94	0.72	11.93	2.27	0.64	2.04	1.47	100.00
Spectrum 3	Yes	62.16		1.54	2.28	15.37	0.85	12.07	1.36	0.53	2.51	1.32	100.00
Max.		62.62	1.34	1.54	2.28	15.42	0.85	12.20	2.27	0.80	2.51	1.47	
Min.		61.66	1.34	0.77	2.01	14.94	0.72	11.93	1.36	0.53	2.04	1.32	

b)

Figure 19 a) FESEM semi quantitative analysis for precipitate at pH = 3.7 (a) and pH = 4.8 (b) respectively. All results in w%

The results for the precipitate at pH 3.7, exposed in Figure 19 *a)*, showed that Fe and O formed the 88 % of the solid. This was also reflected by Hydra-Medusa in Figure 18 *a)*, as the software aimed to the formation of Fe_2O_3. Moreover, Al, Mg and Ca also appeared in a small percentage, which was in concordance with the ICP results.

In a similar manner, the results for the precipitate at pH 4.8, displayed in Figure 19 *b)*, exhibited that Fe was no longer part of the solid, while Al, S and O formed the 89 % of the precipitate. Again, Hydra-Medusa predicted the formation of a compound formed mainly by those elements, as can be observed in Figure 18 *b)*. In addition, Cu and Zn represent the 2.5 % and the 1.4 % of the solid respectively, which is also in concordance with the ICP results.

In conclusion, 100% Fe and 90% Al removal were achieved successfully at pH = 4.8 while target metal loss (Zn and Cu) was below the 10% of the inlet concentration.

3.3. Batch experiments for resin and pH evaluation

The results of the pH screening for each resin will be discussed below. The study has been arranged by the composition of the water in terms of removed metals applying the pre-treatment steps to the sample water.

3.3.1. Real water samples

The first set of displayed results correspond to the equilibrium data after 2 h for the studied resins in contact with an untreated real water sample, that is, no metals were removed from the water.

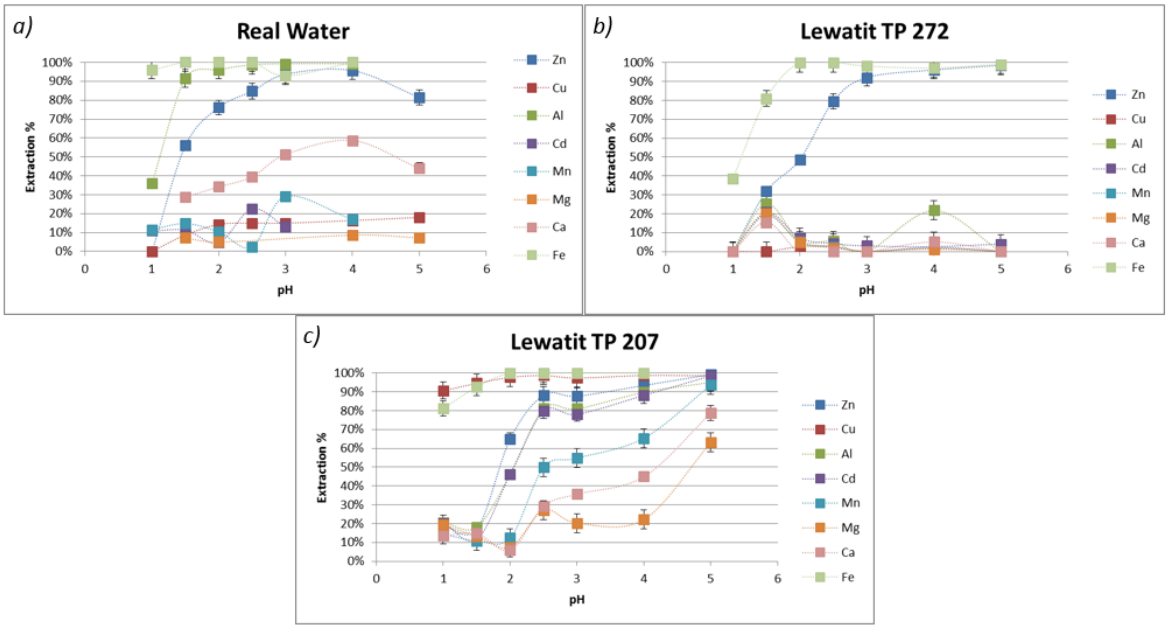

Figure 20 Equilibrium data for resins a) Lewatit VP OC 1026 b) Lewatit TP 272 c) Lewatit TP 207 with real water (containing all metals).

Batch results for resin VP OC 1026, displayed in Figure 20 *a)*, showed that the main competitors for Zn extraction were Fe and Al over the studied pH range. Extraction results were consistent with the selectivity information provided by Lanxess in the product datasheet, which are also available in Table 2. Both, results and the provided information, highlighted Zn selectivity against Mg and Ca, which were the other two major components of the sample. In addition, it was considered that Zn selectivity could be improved by removing both Fe and Al. Taute, Sole, and Hardwick (2013) also observed greater Fe selectivity regarding Zn and remarked the importance of controlling Fe traces due to the difficulty to extract Fe(III) from the resin.

Next, at the right side, the results for resin TP 272 are shown in Figure 20 *b)*. It can be remarked that this resin displayed great selectivity for Zn. However, Fe extraction was predominant for highly acidic pH similar than resin VP OC 1026 (pH < 2). Notice that neither TP 272 nor VP OC 1026 showed good results for Cu adsorption, while Zn preference was clearly observed.

For TP 207 resin, the batch extraction curves are presented in Figure 20 *c)*. Following the same trend as the other resins, Fe was completely extracted over the pH range studied. However, TP 207 was the only resin to show great selectivity for Cu, as the extraction percentage was above 90% for all the studied pHs. As can be observed in Figure 20 *c)*, Cu and Fe were main competitors. Results also indicate that Zn extraction must be taken into account for pH > 2.5.

3.3.2. Real water without Fe samples

The next step was to evaluate the changes to the adsorption equilibrium once Fe, a major competitor has been removed from solution. The pH range studied was from 1 to 3.

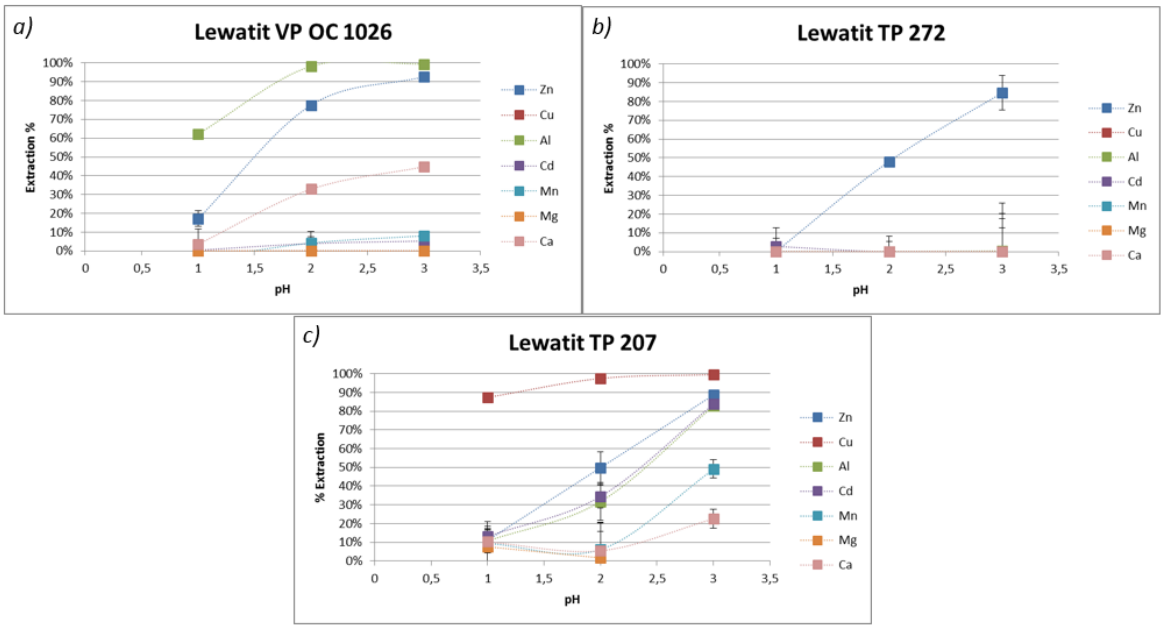

Figure 21 Equilibrium data for resins a) Lewatit VP OC 1026 b) Lewatit TP 272 c) Lewatit TP 207. Iron removed from water samples

The analysis showed that for VP OC 1026 resin, the removal of Fe improved by a 10% the removal capability of Zn and Al at pH > 2, as can be observed from Figure 21 *a)*, although the resin still showed higher Al selectivity.

Following, at the right side, the results for TP 272 are displayed in Figure 21 *b)*. Zn removal improved by a 5% at pH 3 after the removal of Fe. In addition, no extraction of the other metals was observed.

However, for resin TP 207, the removal of Fe did not suppose a significant improvement on the extraction of other ions, as can be seen in Figure 21 *c)*.The removal of Fe increased the resin exchange capacity and the overall extraction rates should improve. It is also important to remark that extraction rates for Al greatly increased with the pH, reaching 80 % for pH > 3.

3.3.3. Real water without Fe and Al

Closing this section of batch experiments, the results for samples without Fe and Al are presented below.

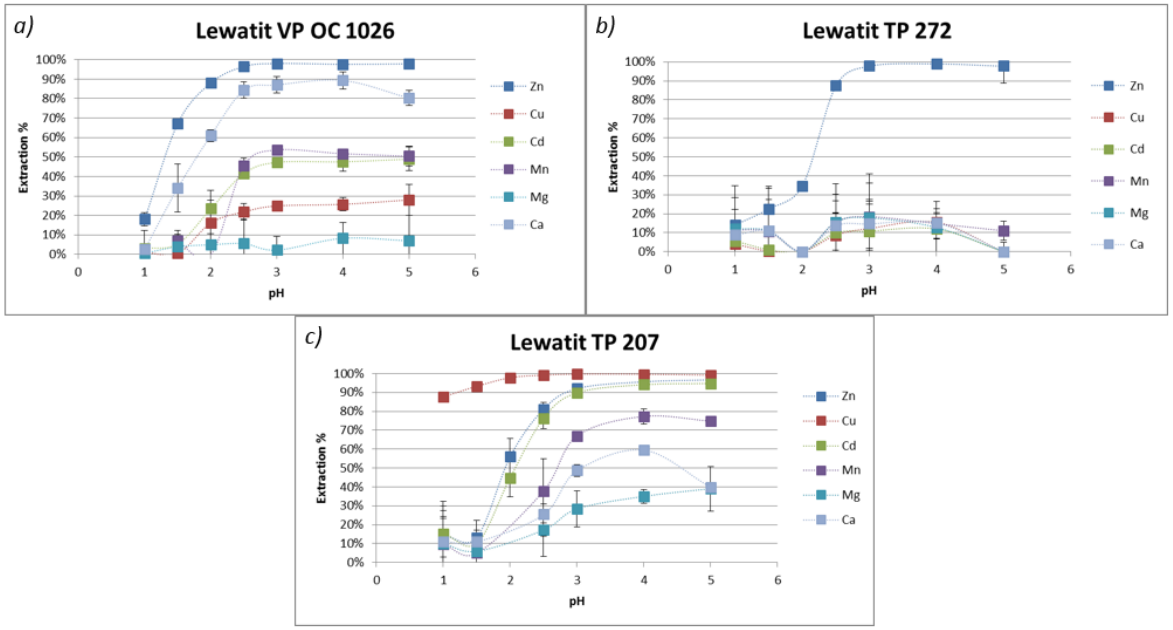

Figure 22 Equilibrium data for resins a) Lewatit VP OC 1026 b) Lewatit TP 272 c) Lewatit TP 207. Fe and Al removed from water samples.

Observing the results for resin VP OC 1026 depicted in Figure 22 *a)*, there was a clear trend for the improvement of Zn extraction once Fe and Al were removed. Complete Zn extraction occurred at pH > 2.5, while Cu extraction remained below the 30 %. This fact made this resin the most suitable for Zn extraction. A process window for column feed pH was established between 2.6 and 2.8 in order to keep extraction of other metals below the 50 %. Simpson and Laurie (1999) and Taute, Sole, and Hardwick (2013) also demonstrated higher selectivity for Zn by VP OC 1026 in the pH window of 1.8 to 3.1.

Resin VP OC 1026 was preferred over TP 272 although Zn extraction rate was maximum (100%) at pH > 3. The main unfavorable factor was that the results obtained from all experiments were considered non conclusive for the other metals. The trend obtained from Figure 20 *b)*, Figure 21 *b)* and Figure 22 *b)* reflected that TP 272 was only Zn selective, as none of the other metals was removed. However, Al and Cu extraction was expected based on the selectivity information provided by Lanxess (Fe(III)>Zn>Al>Cu>Co>Mg>Ca>Ni).

Finally, resin TP 207 presented a solid extraction trend through all experiments. As depicted in Figure 22 *c)*, maximum Cu extraction took place at pH > 3. However, Zn extraction was also favored at high pH, being of 90% when pH > 3. It was the only resin that presented excellent selectivity for Cu. Batch data corresponded with the studies carried out by Valverde et al. (2004) as resin extraction capacity increased with the pH. In addition, selectivity order exhibited at 25 ºC was Cu>Zn>Cd, which verified the results obtained in the pH screening.

Therefore, it was selected for the adsorption of Cu in the column stage. Due to this resin was able to extract both target ions (Zn and Cu), Zn adsorption stage must take place first in the process to reduce the amount of Zn that goes into second column (Cu adsorption).

As summary, the removal of both Fe and Al caused an increase in the extraction capacities of the studied resins. Therefore, the column experiments were carried out with Real water without Fe and Al. Furthermore, Zn separation was performed with VP OC 1026 resin working at pH between 2.6 and 2.8, and Cu separation was performed with TP 207 resin working at pH range from 3 to 4.

Aquí en un 2 frases tiene que quedar claro el agua real que se va emplear, y tipo de resina junto con el pH seleccionados (para cada metal) para hacer experimentos en columnas.

3.4. Bed volume and porosity determination

To determine the column porosity, and consequently the conversion to bed volume, the experimental procedure detailed in 2.6.1 is applied for both, Zn and Cu, columns. NaCl 0.05 M conductivity curves for Zn and Cu columns are displayed in Figure 23 *a)* and Figure 23 *b)* respectively.

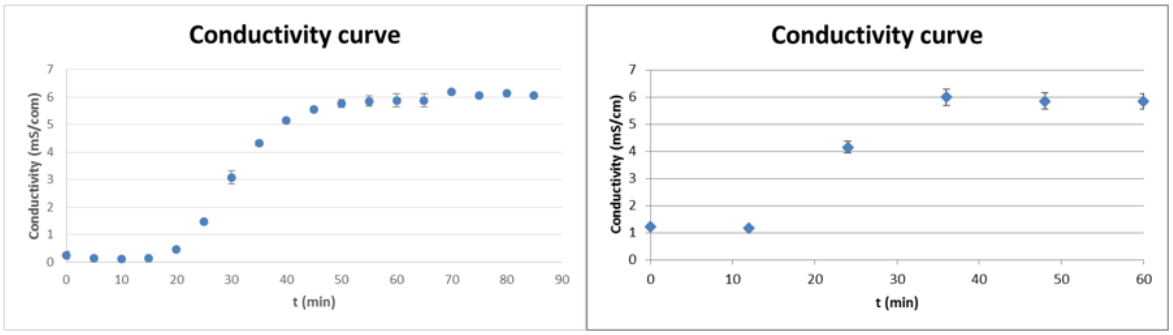

Figure 23 Conductivity curve for a) Zn column and b) Cu column respectively

Once the curves are obtained, the inflection point, $t_{1/2}$, is determined for each column. Applying equations (11), (12) and (13), the relation between column parameters and BV is established, and therefore, curves can now be expressed as a function of a non-dimensional parameter.

Column parameters and calculation results are summarized in Table 5.

	Zn Column	Cu Column
Internal diameter (cm)	2.5	1.1
Column height (cm)	13	7.5
Column volume (mL)	63.81	7.13
Bed length (h_b) (cm)	11	5
$t_{1/2}$ (min)	30	24
Flow rate (ml/min)	1	0.25
Pore volume (mL)	28.75	6
Porosity (ε)	0.45	0.84
Bed volume (V_b) (mL)	24.33	3.31

Table 5 Column parameters and calculation results for Zn and Cu columns

In conclusion, for the Zn column 1 ml/min was equivalent to 2.45 BV/h, and for the Cu column 1 ml/min was equivalent to 18.15 BV/h.

3.5. Ion exchange column results (I): Zn column

The results obtained during the operation with the Zn column will be discussed below.

3.5.1. Preliminary experiment

In order to determine the time needed to reach complete saturation of the column (Zn concentration must be equal to the feed Zn concentration), a preliminary adsorption experiment was carried out.

Real water samples were pretreated to remove both Fe and Al by the process described in 2.3. Average feed composition is displayed in Table 6. Feed pH was 2.68 ± 0.01.

Concentrations in mg/L

Zn	Cu	Al	Cd	Mn	Mg	Na	Ca
771.32 ±25.84	271.67 ±13.00	21.70 ±0.87	2.04 ±0.04	195.79 ±14.27	1976.73 ±122.42	1114.63 ±68.28	496.10 ±10.94

Table 6 Average feed composition for Zn adsorption

The flow rate was set to 6.4 BV/h and the feed pH was adjusted to 2.7.

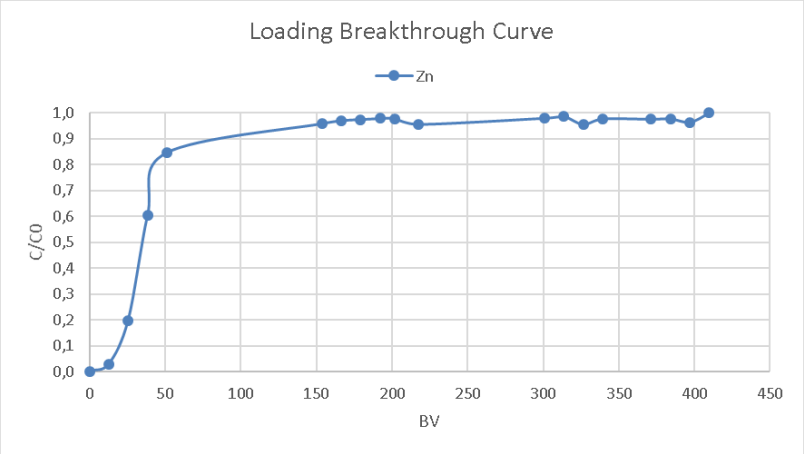

Figure 24 Zn adsorption breakthrough curve of the preliminary test

The breakthrough curve for Zn is represented in Figure 24. The breakpoint and the saturation point were selected as the 20% and 80% of the initial Zn concentration respectively. Therefore, the breakpoint was achieved after 25.6 BV, which is equivalent to 4 h. Moreover, complete saturation of the column was reached in 150 BV (24 h). Therefore, following experiments will be reduced to 24 h. In addition, it was decided to lower the flow rate to 5 BV/h due to system limitations.

After the adsorption cycle, the column was eluted with a 100 g/L H_2SO_4 for 4 h at a flow rate of 2.45 BV/h (1 ml/min). Then, column rinsing with Milli-Q water at elution flow rate took place during 24 h.

3.5.2. Zn adsorption breakthrough curves

The results for adsorption cycles 1 to 4 are displayed in Figure 25. Experiments were carried out at 5 BV/h and the pH of the feed was adjusted to 2.7.

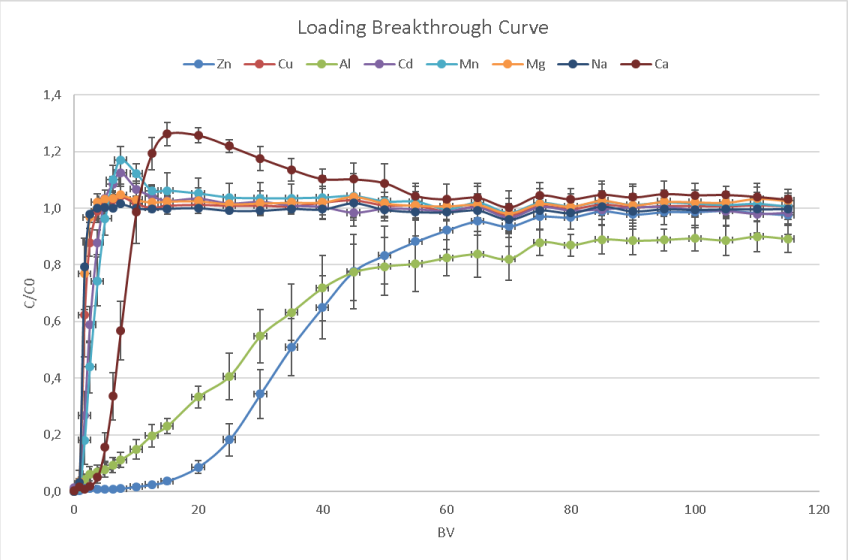

Figure 25 Zn adsorption breakthrough curve (n = 4). Conditions: Flow rate: 5 BV/h; 771 mg Zn/L; pH = 2.7

Figure 25 describes the concentration variation for the different metallic species present in solution. Y-axis expresses the non-dimensional outlet metal concentration in reference to the feed concentration.

The curves shown the selectivity preference of Lewatit VP OC 1026 (Ti>Fe(III)>In>Sn>Sb>Bi>Vo>Be>Al>**Zn**>Pb>Cd>Ca>Mn>Cu>Fe(II)>Co>Ni>Mg>Cr>Alkali). It is visible that the resin predominantly extracted Zn and Al, which was in clear concordance with the results obtained in the batch pH screening in 3.3. Elements with lower extraction preference, in this case Cu, Cd, Mn, Mg, Na reached inlet concentration (C/C_0 =1) within the first 2.5 BV (30 min) of adsorption. Ca adsorption was slightly more favored than the aforementioned metals as saturation was achieved at 10 BV. Although Al was not completely removed in the pretreatment, the remaining concentration was reduced an order of magnitude (around 22 mg/L instead of 363 mg/L), therefore Zn loading was less hindered by this competitor.

Breakthrough point for Zn was achieved after 25 BV (5 h), and saturation, after 47.5 BV (9.5 h) of loading operation. The breakpoint establishes the adsorption cycle length, in consequence an elution should be performed every 25 BV for Lewatit VP OC 1026.

Moreover, Figure 25 showed another important effect to take into account. The breakthrough curves of Ca, Cd, Mn presented C/C_0 values greater than 1. Crittenden et al. (2012) attributed this phenomenon to the competitive effects among the ions present in solution, as preferential ions force previously exchanged ions off the resin. This effect was also reported by Zhou et al. (2013) for organic components.

Table 7 contains the adsorbed metal mass (in mg) per gram of resin. The results exhibit the higher selectivity for Zn regarding the rest of the metals.

Capacities in mg metal/ g resin

Zn	Cu	Al	Cd	Mn	Mg	Na	Ca
23.3 ± 2.2	0.4 ±0.06	0.65 ±0.08	0.004 ± 0.001	0.44 ± 0.08	2.3 ± 0.2	1.4 ± 0.3	2.7 ± 0.3

Table 7 Cation capacities for Lewatit VP OC 1026; Resin mass: 30 g

Jha et al., (2007) reported a capacity of 40.6 mg Zn/g resin for VP OC 1026 after treating a solution consisting of 520 mg/L Zn and 54 g/L Cr. In comparison, the capacity obtained after the experiments was nearly the half (23.3 mg Zn/g resin) because the water treated in this project contained a larger amount of competing ions.

3.5.3. Adsorption pH and conductivity curves

In addition, pH and conductivity were measured for the collected fractions during the adsorption experiments. Both magnitudes were represented in front of the Zn adsorption curve.

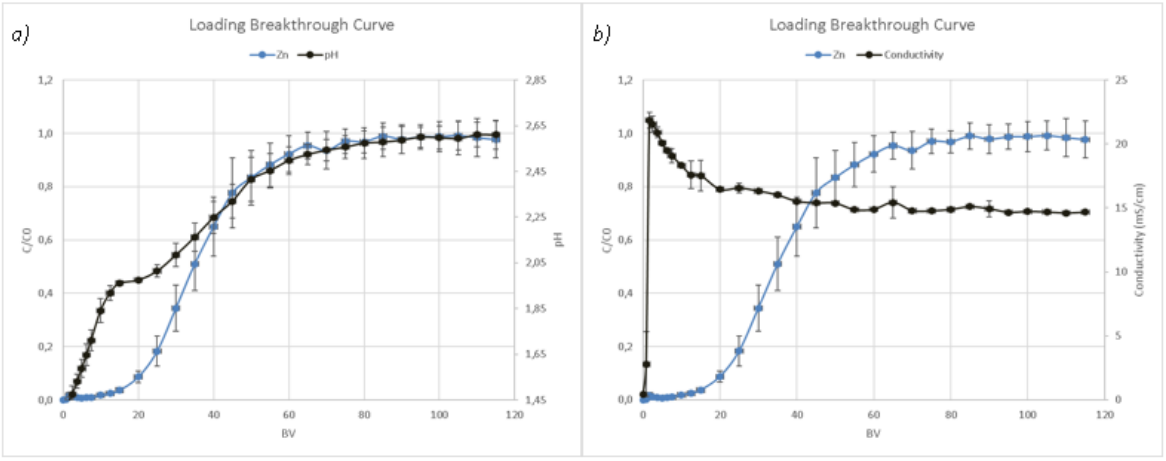

Figure 26 pH curve a) and conductivity curve b) during Zn adsorption (n = 4)

The pH evolution, which can be seen in Figure 26 *a)*¸ was adjusted to the Zn breakthrough curve almost perfectly, especially near resin saturation. Notice that the pH curve followed the adsorption curve in a narrow range, from pH=1.45 to pH=2.65, which was the pH of the feed solution. This behavior could be used to monitor the adsorption process. Inglezakis et al., (2003) also observed the evolution of pH in the absorption of Pb and concluded that acidity in the ion exchange system was influenced by the presence of the adsorbent, but at high Pb concentrations pH was mainly controlled by metals in solution.

It is also remarkable that, during the initial 20 BV, pH curve presented a step in its development, as the initial values rose faster than Zn evolution. This immediate increase occurred while Cu, Cd, Mn, Mg and Ca reached saturation in the resin, as it was shown in Figure 25.

On the other hand, the conductivity curve shown in Figure 26 *b)* did not present any remarkable trend compared to the adsorption curve, as conductivity remained practically constant during the majority of the operation.

3.5.4. Elution profiles for Zn adsorption

Elution cycles were carried out using a 100 g/L H_2SO_4 solution at 2.45 BV/h. The discussion of the results corresponding to the loading cycles that were debated in 3.5.2 is addressed below.

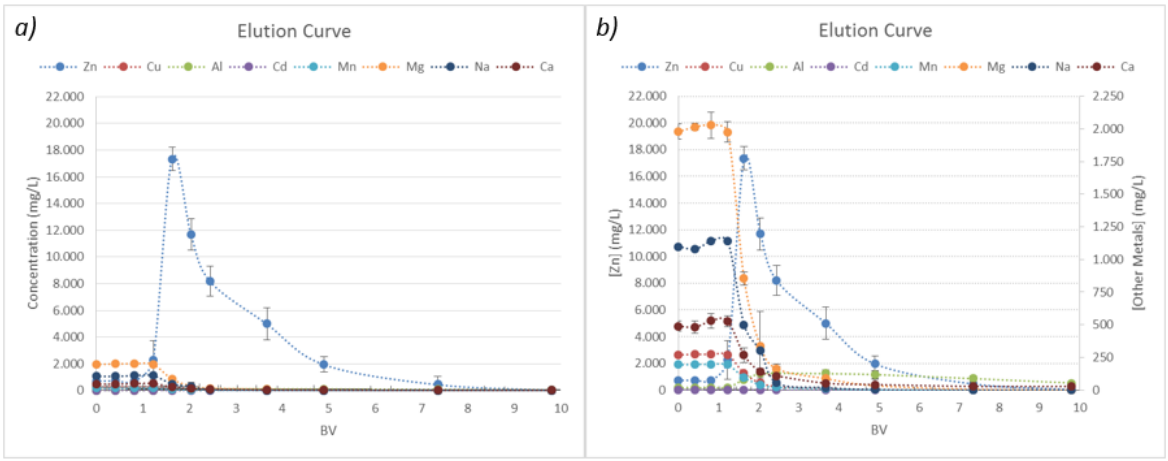

Figure 27 a) General elution profile for Zn column b) General elution profile for Zn column with other metals represented in secondary axis. Conditions: [H_2SO_4]: 100 mg/L; flow rate: 2.45 BV/h. (n=4)

Figure 27 *a)* shows the obtained elution profiles for Zn and the rest of non-target cations. Zn concentration spiked to a maximum of 17392 ± 867 mg/L in the eluate. Elution peak started at 1.23 BV (30 min) and extended until 7.35 BV (3 h). Experimental elution was carried an additional hour in order to ensure the complete peak was obtained.

In Figure 27 *b)* it is observed that before the elution peak appeared, the first 30 min of the elution were required to displace the feed solution that was occupying the column at the end of the adsorption process. Therefore, the concentrations for the other metals were constant or showed very little increase respect the baseline during 1.23 BV.

In order to evaluate the concentration capability of the first column stage, the concentration factors are calculated in Table 8.

Concentration Factor							
Zn	**Cu**	**Al**	**Cd**	**Mn**	**Mg**	**Na**	**Ca**
6.0 ± 1.4	0.3 ± 0.1	4.4 ± 0.9	0.2 ± 0.07	0.3 ± 0.1	0.2 ± 0.1	0.2 ± 0.1	0.3 ± 0.1

Table 8 Concentration factors in Zn separation stage (n = 4)

In the studied conditions, resin VP OC 1026 was able to separate successfully Zn from the other divalent cations, hence concentration obtained in the elution was 6 times the inlet concentration (Zn concentration increased to 4600 mg/L from initially 770 mg/L). On the other hand, the remaining Al from the pretreatment was also concentrated 4.4 times (Al concentration increased to 95 mg/L from initially 21 mg/L).

After the elution operation, the resin was rinsed with Milli-Q water at 2.45 BV/h (1 mL/min) for 18 h.

3.5.5. Elution pH and conductivity curves

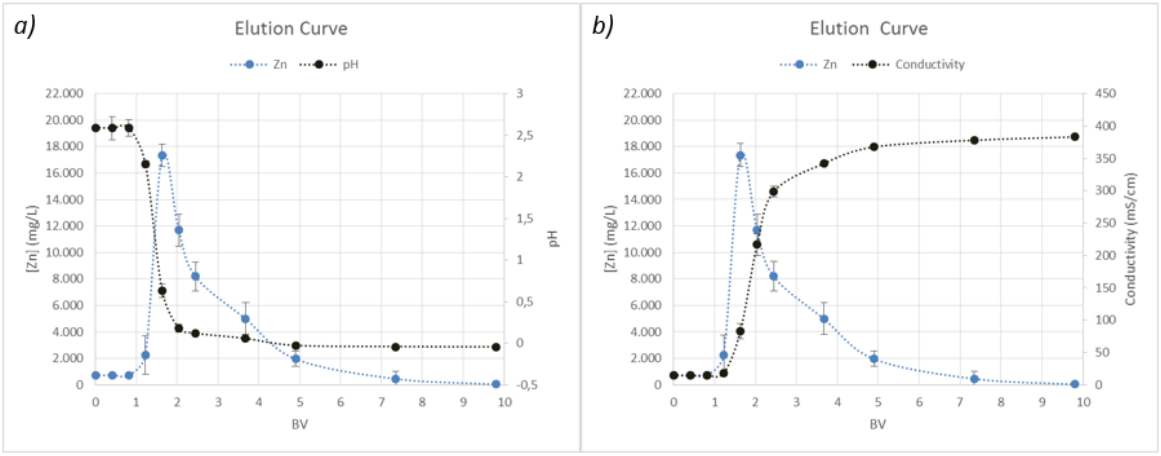

Figure 28 Zn elution pH profile a) and conductivity profile b) Conditions: [H_2SO_4]: 100 g/L; flow rate: 2.45 BV/h. (n=4)

Similarly to the adsorption case (3.5.3), pH and conductivity are contrasted with the Zn concentration during the elution step. Figure 28 *a)* shows the evolution of pH during the operation. It is observed that the pH remains constant until the feed solution has been displaced from the column. Next, it drops to very acidic values once the elution maximum has been passed.

At the same time, Figure 28 b*)* shows the evolution of conductivity during the elution process. In an analogous manner, conductivity remains constant until the feed is displaced out of the column. As the elution advances, more ions are released to the solution, hence the conductivity

increase after the elution peak. In conclusion, both pH and conductivity are useful magnitudes to monitor to control the elution process evolution.

3.5.6. Resin lifetime analysis

The objective of this section is to assess the loss of capacity of VP OC 1026 after the performed experiments. The analysis is performed evaluating the changes produced to the breakthrough and elution curves.

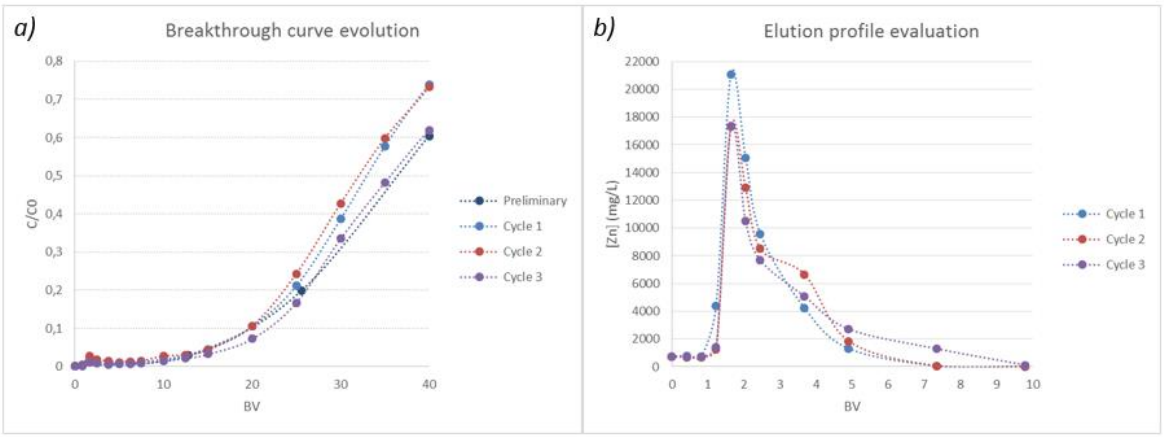

Figure 29 a) Zn breakthrough curves at breakpoint evolution b) Zn elution profile evolution

A loss of capacity is translated in the breakthrough curves as a reduction of the required time, or volume, to reach the breakpoint. In other words, the breakthrough curve “displaces to the left” in the graphics. Loss of capacity is due to the accumulation of cations in the resin due to a degree of irreversibility in the equilibrium reactions.

Therefore, breakthrough curves of the performed adsorption cycles near the breakpoint are shown in Figure 29 *a)*. As it is observed, adsorption curves were primarily close to the value of 20% inlet concentration at 25 BV, which was defined as the breakpoint. Data did not reveal a significant loss of capacity up to this point.

On the other hand, in the elution curves, a loss of capacity is translated to less achieved peak concentration due to the same reasons as the breakthrough. Figure 29 *b)* shows the evolution of the elution profiles. The graphic manifests a decrease in the peak concentration for cycles 2 and 3 compared to cycle 1. However, behavior in cycles 2 and 3 was very similar so the change observed could not be attributed to a loss of capacity with the available data.

Additional studies must be performed to establish a clear trend in the decline of the sorption capacity.

3.6. Ion Exchange column results (II): Cu column

The evaluation of the Cu column is performed in this section, based on a similar approach to the one taken in 3.5.

3.6.1. Preliminary experiment

Feed for Cu experiments is obtained from the effluent of the Zn separation after 5 h operation, that is, until the breakpoint is reached. Inlet concentrations are shown in Table 9.

Concentrations in mg/L

Zn	Cu	Al	Cd	Mn	Mg	Na	Ca
210 ± 33	268 ± 22	5.3 ± 0.6	2.10 ± 0.1	180 ± 16	1844 ± 151	1794 ± 83	426 ± 54

Table 9 Cu column average feed composition (n = 3)

Feed stream was previously adjusted to pH 3.5 to work at maximum Cu extraction rate, in concordance to the results obtained from the batch experiments in 3.3.3 for resin TP 207. The flow rate for the preliminary experiment was 6.17 BV/h (0.34 mL/min).

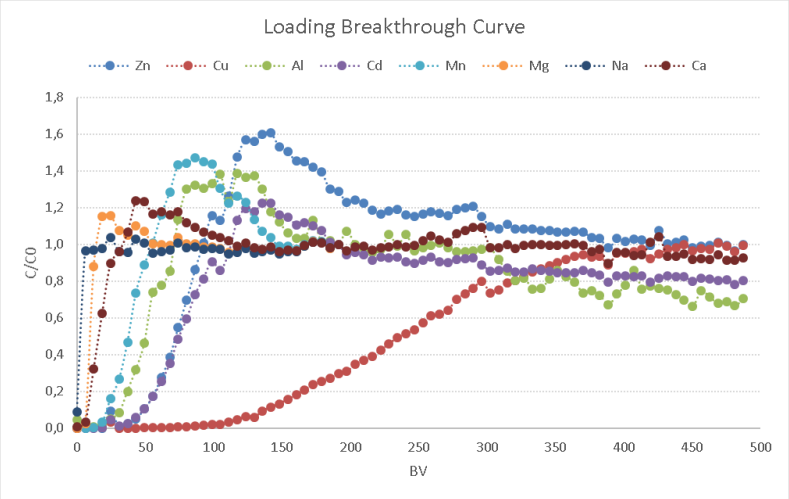

Figure 30 Cu breakthrough curve for the preliminary test. Conditions: Flow rate: 6.17 BV/h; 268 mg Cu/L; pH = 3.5

Figure 30 represents the evolution of metal concentrations in the column effluent for Cu adsorption, expressed as the non-dimensional magnitude C/C_0, that means the outlet concentration divided by the inlet concentration.

The curve showed the selectivity preference of TP 207 as well (**Cu**>VO>UO>PB>Ni>Zn>Cd>Fe(II)>Be>Mn>Ca>Mg>Sr>Ba>Na), in a similar manner to that observed for Zn adsorption in 3.5.2, and also in concordance with the batch results. Complete saturation for Cu was achieved after 444 BV (72 h). In addition, Mg saturated after 18.5 BV (3 h), Ca saturated after 37 BV (6 h), Mn saturated after 55.5 BV (9 h), Al saturated

after 74 BV (12 h), Zn saturated after 92.6 BV (15 h) and finally, Cd saturated after 117.25 BV (19 h). On the other hand, Na was released from the iminodiacetic acid groups of the resin as it was originally conditioned to the basic form.

Although the outlet effluent of the Cu column is not treated further in other column, the breakpoint for the column was set to the 20% of Cu inlet concentration. Breakthrough point was achieved after 166.6 BV (27 h) in the preliminary test.

Figure 30 also showed values of C/C_0 greater than 1 for Zn, Al, Cd, Mn, Mg, Na and Ca, as described by Crittenden et al. (2012) and Zhou et al. (2013). However, the effect for this column may be greater due to the release of Na^+ from the resin functional groups as the extraction of water pollutants advances.

The elution of the column was carried out afterwards at 2.9 BV/h (0.16 ml/min) with H_2SO_4 100 g/L during 10 h. Following, the resin was conditioned back to the alkali form regenerating with 1 M NaOH solution at elution flow rate solution during 1 h 45 min, until pH and conductivity stabilized. Finally, resin bed was rinsed with Milli-Q water at 6.2 BV/h during an hour (slow cleaning), followed by another rinse at 18.15 BV/h (quick cleaning) for 24 h.

3.6.2. Cu adsorption breakthrough curves

In the preliminary test, Cu saturated after 72 h of adsorption. In order to decrease the duration of the adsorption process to around 24 h, it was decided to increase the flow rate from 6.17 BV/h (0.34) to 24.68 BV/h (1.36 ml/min).

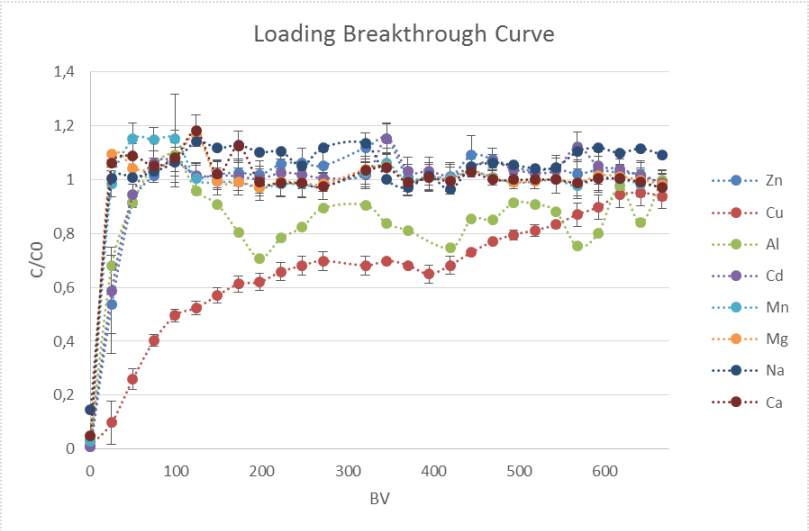

Figure 31 Cu breakthrough curve (n = 3). Conditions: Flow rate: 24.68 BV/h; 268 mg Cu/L; pH = 3.5

Figure 31 represents the breakthrough curve at the new flow rate conditions. As expected, Cu saturation was achieved after 617 BV (25 h). Although the time to reach complete saturation

decreased, the difference in BV respect to the preliminary test was due to difficulties during the operation of the fast cycles. The rest of the ions saturated in less than 24.7 BV (1 h).

Comparing the preliminary test curve (Figure 30), and the adsorption curves represented in Figure 31, the effect of the flow rate on the shape of the breakthrough curves described by Ghorai and Pant (2005) could be observed, as the curves for all ions became steeper after increasing the flow rate from 6.17 BV/h to 24.68 BV/h.

As mentioned above, the breakthrough point was defined as the 20% of the inlet Cu concentration. Breakpoint was reached after 37.7 BV (3.84 h). Therefore, elution must be carried out after 3.84 h of adsorption.

Table 10 contains the resin capacity for each studied cation, expressed as extracted metal mass divided by resin mass.

Capacities in mg metal/ g resin

Zn	Cu	Al	Cd	Mn	Mg	Na	Ca
4.5 ± 1.1	37.8 ± 2.1	0.2 ± 0.1	0.1 ± 0.1	5.1 ± 0.3	13.6 ± 0.7	4.7 ± 0.2	5.2 ± 0.3

Table 10 Capacities for Lewatit TP 207. Resin mass: 4 g

Results reflect higher selectivity for Cu extraction regards the rest of the metals, as the resin was able to extract 38 mg of Cu per gram of resin, which is 3 times the registered capacity for Mg and 8 times the capacity for Zn, which were major competitors in the pH range selected in batch experiments.

The obtained Cu capacity was lower than the reported by Park, Parhi, and Kang (2012), which was 68.7 mg Cu/g resin when treating a solution containing 512 mg/L Cu, 212 mg/L Fe, 15.16 g/L Ni and 2 g/L Co, as a consequence of a pre-treatment done to the resin for swelling the polymeric matrix, enhancing the performance.

3.6.3. Adsorption pH and conductivity curves

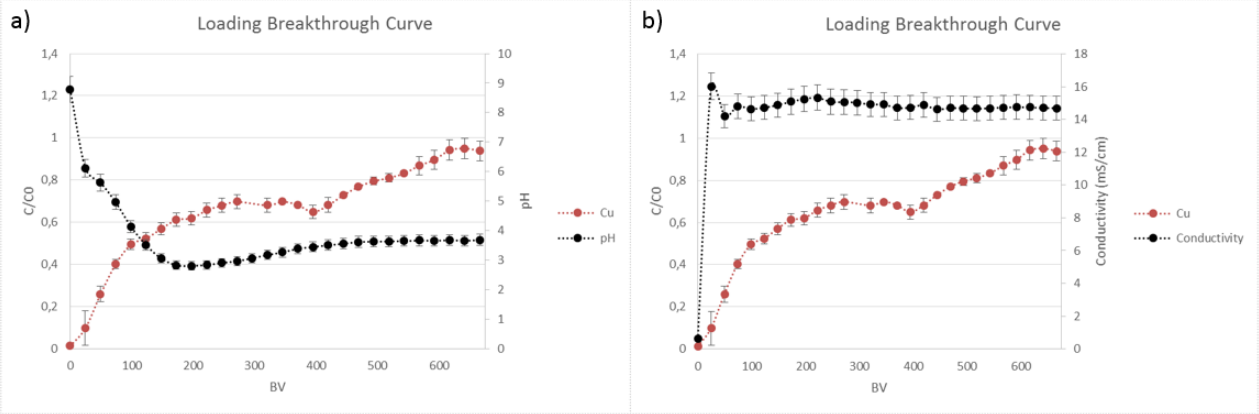

Figure 32 pH curve a) and conductivity curve b) during Cu adsorption

The evolution of pH and conductivity was represented over the Cu adsorption. The pH curve, shown in Figure 32 *a)*, experimented a rapid decrease. Initial pH of the resin was basic because of the conditioning with NaOH required to convert the resin functional groups to the working form (Na^+ form) prior to every adsorption cycle. After rinsing for 24h after the conditioning, the resin was still buffered. No clear relation between pH and the adsorption curve shape could be established. Therefore, pH was not a suitable magnitude for monitoring the process. In this case, the effects described by Inglezakis et al., (2003) were barely noticeable.

Figure 32 *b)* shows the conductivity curve represented over the adsorption curve. It is observed that conductivity remained constant during the whole process, with exception of an initial peak, while the resin was releasing Na^+ from its initial form. In conclusion, conductivity tracking is not appropriate for adsorption monitoring.

3.6.4. Elution profiles for Cu adsorption

The elution of the Cu ions from the resin was carried out with a 100 g/L H_2SO_4 solution at a flow rate of 13.1 BV/h (0.72 ml/min). Elution profiles are represented in Figure 33.

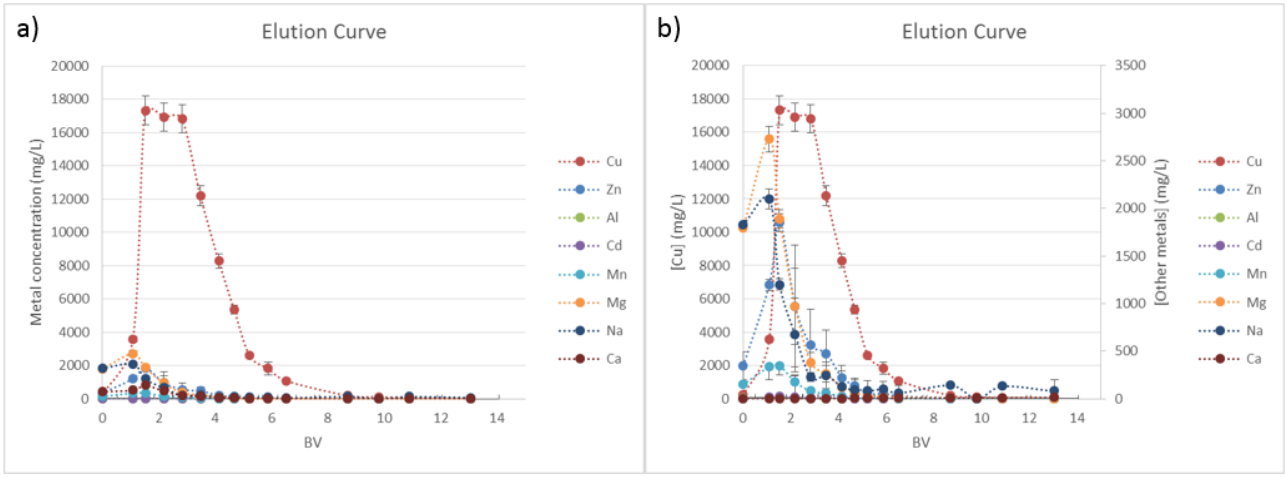

Figure 33 a) General elution profile for Cu column b) General elution profile for Cu column, other metals represented in secondary axis. Conditions: [H_2SO_4]: 100 g/L; flow rate: 13.1 BV/h (n=3)

Figure 33 *a)* shows the obtained elution profiles. Cu concentration achieved a maximum value of 17323 ± 866 mg/L in the eluate. Elution peak started at 1.52 BV (7 min) and extended until 8.71 BV (40 min).

In Figure 33 *b),* it is observed that the first 5 min of the elution were required to displace the feed solution that was occupying the column at the end of the adsorption process.

In order to evaluate the concentration capability of the second column stage, the concentration factors are shown in Table 11.

Concentration Factor							
Zn	**Cu**	**Al**	**Cd**	**Mn**	**Mg**	**Na**	**Ca**
0.6 ± 0.1	25.1 ± 2.9	0.6 ± 0.3	1.7 ± 0.7	0.4 ± 0.1	0.2 ± 0.1	0.2 ± 0.1	0.4 ± 0.1

Table 11 Concentration factors in Cu separation stage

In the studied conditions, TP 207 proved to be an excellent resin for Cu separation and concentration. As the results show, the Cu concentration factor was 42 times greater than Zn and 125 times than Mg, which were the major competitors in the selected pH window.

After the elution, the resin bed is slowly conditioned with a NaOH 1 M solution at a flow rate of 2.9 BV/h during 1 h 45 min. Resin conditioning was assumed concluded when both pH and conductivity exiting the column were stable. Then prior to the next adsorption cycle, the resin is rinsed with Milli-Q water at 6.2 BV/h during an hour (slow cleaning), followed by another rinse at 18.15 BV/h (quick cleaning) for 24 h.

3.6.5. Elution pH curve

Additionally, pH curve was compared to the elution curve in order to look for a magnitude that allowed the monitoring of Cu adsorption process.

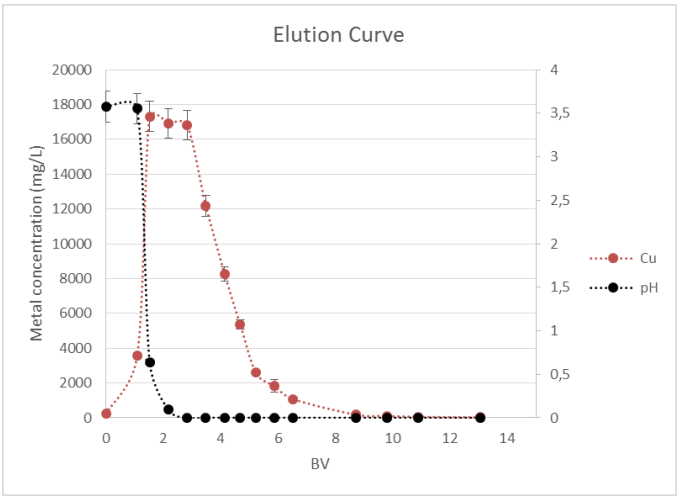

Figure 34 Zn elution pH profile: [H_2SO_4]: 100 mg/L; flow rate: 2.90 BV/h.

Figure 34 describes the pH curve over the Cu elution. It can be observed that the pH presented a similar behavior to that exposed in 3.5.5 during the Zn elution cycles: pH remained constant while the feed solutions were not displaced. Then it rapidly decreased to very acidic values (pH=0). While this observation was useful for the first bed volumes, the curve did not provide information about the end of the Cu peak.

3.7. Preliminary study on electrowinning

Three batch experiments were carried out to study the behavior of the parameters involved in the deposition of Zn and Cu from the elution streams obtained in column operation. The applied current intensities, for the experiments are shown in Table 12.

	Zn	*Cu*
R1	4.09 A	0.53 A
R2	7.13 A	1.06 A
R3	10.03 A	2.12 A

Table 12 Applied current intensities for each electrowinning test

The electrodes were a 12x12 cm AISI 304 stainless steel cathode, with 288 cm^2 of effective surface, and two 10x10 cm IrO_2 coated Ti anodes, with an effective surface of 320 cm^2. Separation between cathode and anodes was 2 cm.

First, the evolution of the input current intensity, and the resulting electric potential for each elution stream are studied in Figure 35 *a)* and Figure 35 *b)*.

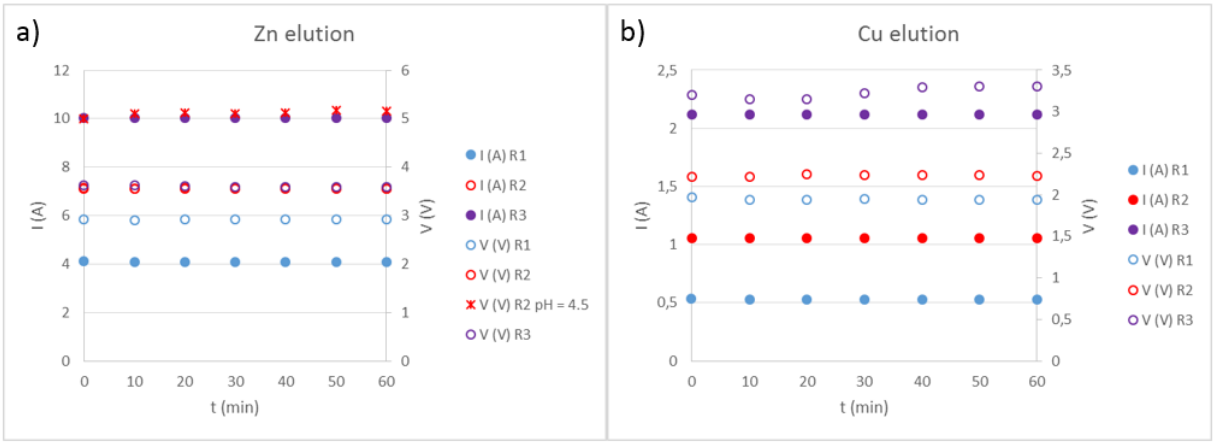

Figure 35 a) Current intensity and electric potential during Zn deposition b) Current intensity and electric potential during Cu deposition

Observing both, Figure 35 *a)* and Figure 35 *b)*, it is visible that current intensity and the resulting potential were constant during the experience. Panda and Das (2001) observed this behavior with Ti-IrO_2 oxide anodes when studying the electrowinning of Cu from acidic sulfate solutions. In addition, the resistance of the cell was also constant as a consequence of Ohm's law. According to Gamburg and Zangari (2011), the ohmic resistance of the solution can be approximated by the inverse of the electrolyte conductivity. Electrical conductivity of the solution remained constant at 272 mS/cm during the experiments. Therefore, the ohmic relation was confirmed.

Following, the removal % of Zn and Cu from the liquid phase was evaluated by AAS. Results for the Zn elution stream were represented in Figure 36 *a)* and Figure 36 *b).*

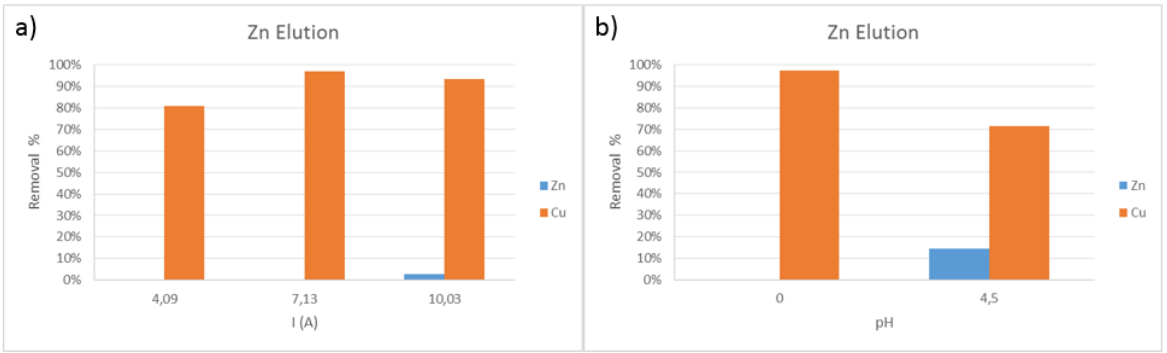

Figure 36 a) Zn and Cu removal % from the Zn-rich stream at pH = 0, Intensities: 4 A, 7 A, 10 A
b) Zn and Cu removal % from the Zn-rich stream at 7 A, pH: 0 and 4.5

Figure 36 *a)* shows the removal % for both target metals at pH = 0 for all three intensities tested. It was observed that Cu deposition was predominant, being always superior to the 80%. The maximum reported was 97% Cu removal and occurred at 7.13 A. In the experiment

performed at 10.03 A, it was noticed that the 3% of Zn was removed from solution in addition to a minor decrease (3%) of the Cu removal reached at 7.13 A. Therefore deposits obtained at pH = 0 were all similar to the one presented in Figure 37 *a)*. The color of the metal layer evidenced that Cu deposition was predominant.

Salles et al. (2011) observed an increase in Zn deposition efficiency after increasing pH from 2 to 4, as the formation of a first layer of Zn on the electrode surface rapidly improved the growth of the Zn layer. In addition, the work of other authors in the field of Zn alloys, such as Beltowska-Lehman et al. (2002) and Winiarski et al. (2016) also showed improved results between pH=4 and pH=6. Therefore, another experiment, increasing the pH to 4.5 was carried out at 7.13 A.

The effect of the pH is shown in Figure 36 *b)*. In this case, working at pH=4.5 resulted in the removal of the 15% of Zn. Similarly, Figure 37 *b)* shows the deposit obtained from the Zn-rich solution at 7 A and pH = 4.5.

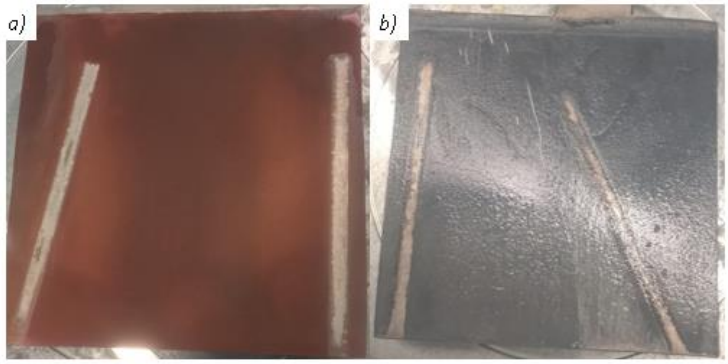

Figure 37 a) Deposited layer at pH = 0 b) Deposited layer at pH = 4.5

The experimented color change could be a consequence of the deposition of a Zn layer. Therefore, to verify Zn deposition, a sample from the metal layer generated on the cathode was analyzed by FESEM, pictured in Figure 38 *a).*

a)

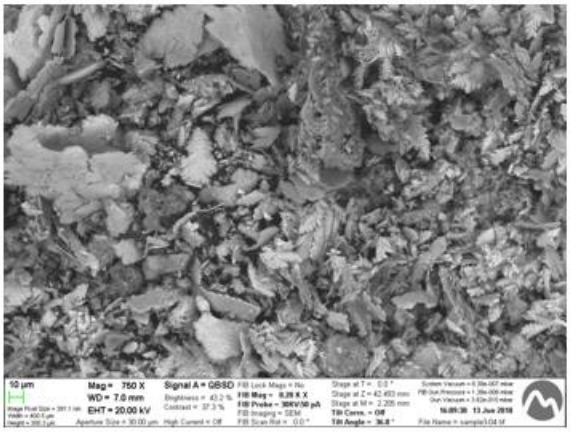

b)

Spectrum	In stats.	O	Mg	Al	S	Cl	Zn	Total
Spectrum 1	Yes	19.57	2.27	0.28	3.22	0.90	73.76	100.00
Mean		19.57	2.27	0.28	3.22	0.90	73.76	100.00
Std. deviation		0.00	0.00	0.00	0.00	0.00	0.00	
Max.		19.57	2.27	0.28	3.22	0.90	73.76	
Min.		19.57	2.27	0.28	3.22	0.90	73.76	

Figure 38 a) FESEM image of the deposit at 7 A, pH = 4.5 *b)* Semi quantitative analysis results

A semi quantitative analysis was carried out to determine the composition of the solid. Results, shown in Figure 38 *b)*, determined that Zn represented the 74% of the deposit. Mg and Al also deposited during this process, representing the 2.3% and 0.3% respectively. Cu, on the other hand, was not detected in the sample.

Results obtained after 1 h for an equivalent current density of 223 A m^{-2} (7.13 A in 320 cm^2 anodic surface) at pH=4.5, were similar to Simpson and Laurie (1999), who reported a 78% Zn composition after electrowinning applying a current density of 100 A m^{-2} in 4 hours for a solution at pH=1.8. Therefore, increasing current intensity and pH resulted in a reduction of the time needed to achieve a determined deposit quality.

In relation to the Cu elution stream experiments, Figure 39 shows the removal % for both, Zn and Cu.

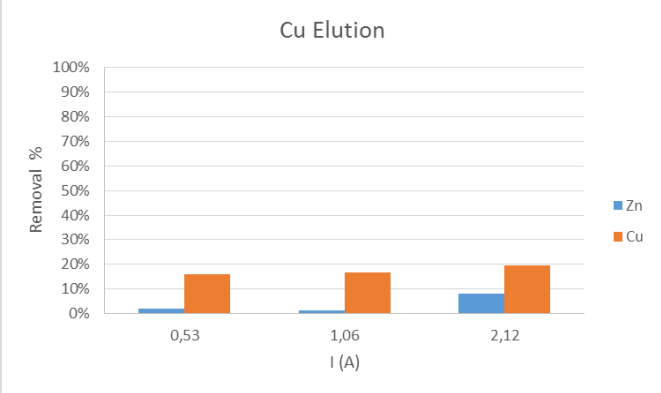

Figure 39 Zn and Cu removal % from the Cu-rich stream at pH = 0, Intensities: 0.5 A, 1 A, 2 A

The results showed little evolution on the Cu removal, as it ranged from 16% at 0.5 A to 19% at 2 A. Maximum Zn removal, which was around the 8%, was also achieved at 2 A.

Deposits obtained after the experiments at 0.5 A and 2 A were also analyzed by FESEM. Small metallic particles, depicted in Figure 40 *a)* were obtained at 0.5 A. Therefore, a section of it had to be selected, as shown in Figure 40 *b)*, in order to perform the analysis.

a)

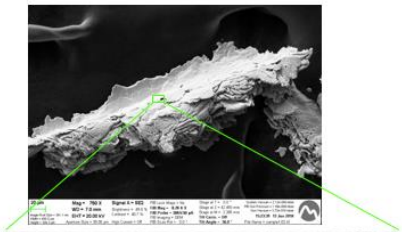

b)

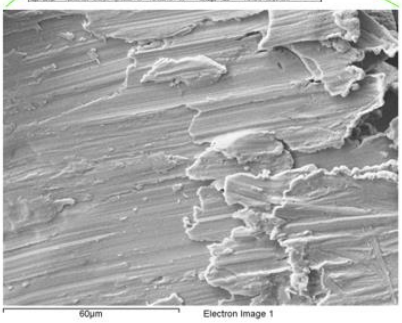

c)

Spectrum	In stats.	C	O	Fe	Cu	Total
Spectrum 1	Yes	3.73	0.67	0.58	95.02	100.00
Mean		3.73	0.67	0.58	95.02	100.00
Std. deviation		0.00	0.00	0.00	0.00	
Max.		3.73	0.67	0.58	95.02	
Min.		3.73	0.67	0.58	95.02	

Figure 40 a) FESEM image of a particle obtained at 0.5 A b) Selected surface of the particle c) Semi quantitative analysis results

Semi quantitative analysis over the selected surface, shown in Figure 40 *c)*, exposed that Cu, which represented 95% of the total mass, mainly formed the deposit. Trace levels of Fe (0.6%) are present in the sample may be due to the sample manipulation. Zn was not detected in the sample.

In contrast, the collected sample at 2 A was as metallic powder. The FESEM image of the sample can be observed in Figure 41 *a)*.

a)

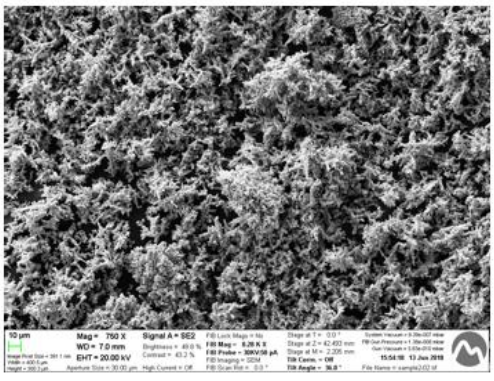

b)

Spectrum	In stats.	C	O	S	Cu	Total
Spectrum 1	Yes	12.08	6.33	0.40	81.19	100.00
Mean		12.08	6.33	0.40	81.19	100.00
Std. deviation		0.00	0.00	0.00	0.00	
Max.		12.08	6.33	0.40	81.19	
Min.		12.08	6.33	0.40	81.19	

Figure 41 a) FESEM image of the simple obtained at 2 A b) Semi quantitative analysis results

Similarly, semi quantitative analysis results are shown in Figure 41 *b)*.As in previous case, Cu, which represented the 81% of the total mass, was the main element of the deposit. However, a small amount of S (0.4%) was also found in the sample.

Gravimetric analysis, however, displayed in Figure 42 *a)* and *b)* revealed quite limited mass gain on the electrodes.

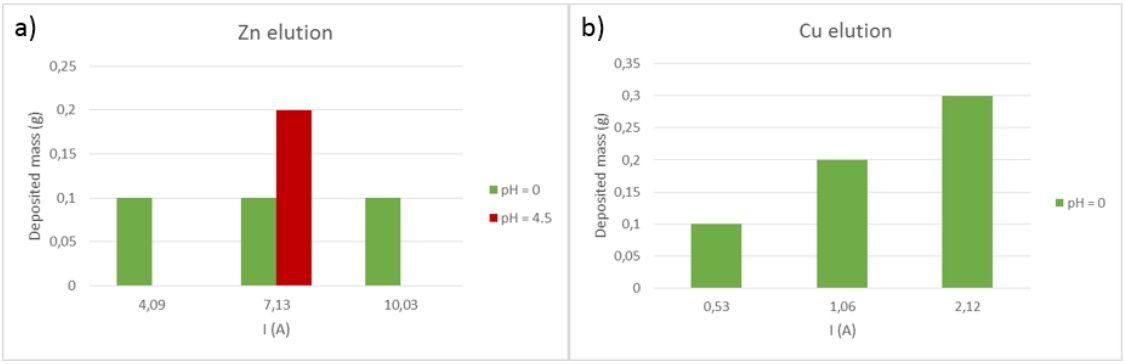

Figure 42 Gravimetric analysis for Zn (a) and Cu (b) deposition respectively

Figure 42 a*)* shows that, for the Zn deposition, the gained mass remained constant at 0.1 g in all studied intensity range. The increase of deposited mass at 0.2 g was produced at pH=4.5 and 7.13 A. Moreover, the mass gain for the Cu experiments, depicted in Figure 42 *b)*, showed constant increase in each experiment as intensity increases. At the best conditions, the deposited mass was 0.3 g for Cu.

The results of this preliminary test showed that electrowinning could be a feasible solution to the removal of Cu impurities from the Zn elution, being the maximum removal of 97% at 7.13 A and pH=0. However, further studies are required to determine the optimal conditions for the recovery of Cu and Zn.

4. Conclusions

The separation and recovery of Zn and Cu, from a real acidic mine water, as valuable metals was addressed by means of ion-exchange columns. Solvent impregnated resins Lewatit VP OC 1026 and Lewatit TP 272, and the chelating resin Lewatit TP 207 were evaluated to perform the task.

In relation to the batch experiments:

- 100% Fe and 96% Al removal was achieved after chemical oxidation with 1 ml H_2O_2 35% (v/v) per litre of mine water and precipitation at pH=4.8.
- Resin VP OC 1026 was chosen for the separation of Zn as 100% extraction was achieved at pH>2.5. The selected pH operating range was 2.6-2.8, since Cu extraction was 30% in this range, and Cd, Mn, Mg, Na and Ca all remained below the 50% extraction.
- Resin TP 207 was chosen for the separation of Cu due to reaching 100% at pH>3. The selected pH operating range was 3-4. However, the resin presented 80% Zn extraction in that pH range. In consequence, Cu separation was executed after the Zn separation stage.

In relation to the column experiments:

- The breakthrough curves for VP OC 1026 and TP 207 proved the selectivity for Zn and Cu respectively, as both metals were the last to reach saturation.
- Adsorption cycle times were determined by the time to reach the breakpoint. In consequence, adsorption operation time was 5 h (25 BV) for Zn and 3.84 h (37.7 BV) for Cu.
- The capacity of Lewatit VP OC 1026 was 23.27 mg Zn/g resin while the capacity of TP 207 was 36.25 mg Cu/g resin.
- Zn and Cu could be successfully eluted and concentrated with a 100 g/L H_2SO_4 solution. Zn elution is completed after 3 h (7.35 BV), and Cu elution after 4 h (11.62 BV). The concentration factors were 6 and 27 times (the inlet concentration) for Zn and Cu respectively.

In relation to the electrochemical experiments:

- Electrochemical experiments proved successful to remove the 97% of Cu from a Zn rich solution applying 7.13 A during 1 h.
- Mass deposition on cathode surface was little, around 0.1-0.2 g for Cu at pH=0 and Zn at pH=4.5. For that reason, further studies are required to improve the Cu and Zn deposition.

5. Economic evaluation

A small economic evaluation is performed in relation to the aspects relevant to the experimental part.

5.1. Reagents and supplies

Reagent cost is calculated in terms of the consumed amount in Table 13.

Reagent	*Unit cost*	*Amount*	*Costl (€)*
H_2SO_4	30.92 €/L	1.192 L	36.86
H_2O_2	104.6 €/L	0.03 L	3.14
NaOH	30.25 €/kg	0.24 kg	7.26
Lewatit TP 207	212 €/kg	0.1 kg	21.2
Lewatit TP 272	318 €/kg	0.1 kg	31.8
Lewatit VP OC 1026	286 €/kg	0.1 kg	28.6
TOTAL			*128.86*

Table 13 Reagent cost Source: Sigma Aldrich (Spain | Sigma-Aldrich)

In addition the water usage costs are computed below in Table 14:

Concept	*Unit price (€/L)*	*Amount (L)*	*Cost (€)*
De-ionized water	1	20	20
Milli-Q water	1.1	100	110
Total			*130*

Table 14 Water supply cost

5.2. Equipment and analytics

Equipment expenses are computed through amortization costs instead of the instrumental total cost, as the equation (24) expresses. Equipment lifespan was considered of 10 years. Resulting cost is included in Table 15.

$$Amortization = \frac{Instrument\ Cost \cdot Use\ time}{Service\ Life} \quad (24)$$

Concept	*Equipment cost (€)*	*Use time (y)*	*Cost (€)*
Glass column 2.5 cm diameter	302.76	0.5	15.14
Glass column 1.1 cm diameter	1113.17	0.5	55.66
Total			*70.80*

Table 15 Equipment costs Source: Kinesis (Kinesis)

Other equipment that has been used, such as the peristaltic pumps and the fraction collector, are considered fully amortised.

Analysis cost is calculated from the number of analysed samples in Table 16.

Concept	*Unit price (€/u)*	*Amount (u)*	*Cost (€)*
ICP	21.13	706	14917.78
FESEM	15	10	150
Total			*15067.78*

Table 16 Analysis costs

5.3. Personnel

Personnel costs include the salary for a technical chemical engineer, as established in the collective agreement for technical personnel (UGT, 2013) and 2 supervisors. Supervisor salary has been estimated as 2.5 times the technical engineer's salary. Costs are included in Table 17.

Concept	*Unit salary (€/h)*	*Dedication (h)*	*Cost (€)*
Technical CE	15	900	13,500
Supervisor	37.5	120	4,500
Total			*18,000*

Table 17 Personnel costs

5.4. Total cost

Total cost of the project is the sum of the total costs from Table 13, Table 14, Table 15, Table 16 and Table 17. Global expenses are summarized in Table 18.

Concept	*Cost (€)*
Reagents	128.86
Supplies	130.00
Equipments	70.80
Analytics	15,067.78
Salaries	18,000.00
Subtotal 1	33,397.27
VAT (21%)	7,013.46
TOTAL	*40,410.73*

Table 18 Project total cost

The total cost of the project is around 40500 €.

6. Environmental analysis

The present project sets the basis for the implementation of a larger scale system for the treatment and revalorization of acidic mine waters. The experimental part was entirely executed at laboratory scale. Therefore, the main impacts are associated to the proper usage of supplies, for example water, paper and electricity mainly, as well as an appropriate waste management (external service).

However, several issues that must be taken in consideration in larger scale application of the research obtained in this project are:

- Proper management of sludges formed during the chemical precipitation stage in the pre-treatment of the acidic mine water.
- Exhausted resin disposal after exceeding the lifespan of the ionic exchangers.
- Proper management of the acidic waters produced after the rinsing the resin beds.
- Full-scale energy consumption for the electrochemical recovery of the target metals.

References

Achterberg, E.P., Braungardt, C., Morley, N.H., Elbaz-Poulichet, F., and Leblanc, M. (1999). Impact of Los Frailes mine spill on riverine, estuarine and coastal waters in southern Spain. Water Res. *33*, 3387–3394.

Akcil, A., and Koldas, S. (2006). Acid Mine Drainage (AMD): causes, treatment and case studies. J. Clean. Prod. *14*, 1139–1145.

Alexandratos, S.D., and Ripperger, K.P. (1998). Synthesis and characterization of high-stability solvent-impregnated resins. Ind. Eng. Chem. Res. *37*, 4756–4760.

Beltowska-Lehman, E., Ozga, P., Swiatek, Z., and Lupi, C. (2002). Electrodeposition of Zn-Ni protective coatings from sulfate-acetate baths. Surf. Coatings Technol. *151–152*, 444–448.

Cossio, M.L.T., Giesen, L.F., Araya, G., Pérez-Cotapos, M.L.S., VERGARA, R.L., Manca, M., Tohme, R.A., Holmberg, S.D., Bressmann, T., Lirio, D.R., et al. (2012). Ion Exchange Materials Properties and Application (London: Elsevier B.V.).

Crittenden, J.C., Trussell, R.R., Hand, D.W., Howe, K.J., and Tchobanoglous, G. (2012). MWH's Water Treatment: Principles and Design.

Denning, P.C., and Dvorak, B.I. (2009). Maximizing Sorbent Life: Comparison of Columns in Parallel, Lead-Lag Series, and with Bypass Blending. Water Environ. Res. *81*, 206–216.

España, J.S., Pamo, E.L., Santofimia, E., Aduvire, O., Reyes, J., and Barettino, D. (2005). Acid mine drainage in the Iberian Pyrite Belt (Odiel river watershed, Huelva, SW Spain): Geochemistry, mineralogy and environmental implications. Appl. Geochemistry *20*, 1320–1356.

Gamburg, Y.D., and Zangari, G. (2011). Theory and Practice of Metal Electrodeposition (London: Springer).

Garg, B.S., Sharma, R.K., Bhojak, N., and Mittal, S. (1999). Chelating resins and their applications in the analysis of trace metal ions. Microchem. J. *61*, 94–114.

Van Geen, A., Takesue, R., and Chase, Z. (1999). Acid mine tailings in southern Spain. Sci. Total Environ. *242*, 221–229.

Ghorai, S., and Pant, K.K. (2005). Equilibrium, kinetics and breakthrough studies for adsorption of fluoride on activated alumina. Sep. Purif. Technol. *42*, 265–271.

Inglezakis, V.J., and Poulopoulos, S.G. (2006). Adsorption, Ion Exchange and Catalysis: Design of Operations and Environmental Applications (Athens: Elsevier B.V.).

Inglezakis, V.J., Loizidou, M.D., and Grigoropoulou, H.P. (2003). Ion exchange of Pb2+, Cu2+, Fe3+, and Cr3+on natural clinoptilolite: Selectivity determination and influence of acidity on metal uptake. J. Colloid Interface Sci. *261*, 49–54.

Inui, A., Hama, C., Katsuragawa, T., Iwata, S., and Yuchi, A. (2013). Divalent/monovalent selectivities and secondary interactions of multibasic acids on anion exchange resins. Ind. Eng. Chem. Res. *52*, 16880–16886.

Jha, M.K., Kumar, V., and Lee, J.-C. (2007). Processing of electroplating effluent for the recovery of zinc and chromium using ion exchange technique. In TMS Annual Meeting, B. Davis, and M. Free, eds. (The Minerals, Metals & Materials Society), pp. 77–86.

Kabay, N., Cortina, J.L., Trochimczuk, A., and Streat, M. (2010). Solvent-impregnated resins (SIRs) - Methods of preparation and their applications. React. Funct. Polym. *70*, 484–496.

Kammerer, J., Carle, R., and Kammerer, D.R. (2011). Adsorption and ion exchange: Basic principles and their application in food processing. J. Agric. Food Chem. *59*, 22–42.

Kartikaningsih, D., Shih, Y.J., and Huang, Y.H. (2016). Boron removal from boric acid wastewater by electrocoagulation using aluminum as sacrificial anode. Sustain. Environ. Res. *26*, 150–155.

Lanxess (2011a). Lewatit VP OC 1026 Product information. 1–6.

Lanxess (2011b). Lewatit TP 272 Product information. 2–7.

Lanxess (2011c). Product Information - Lewatit® TP 207. 1–5.

Luqman, M. (2013). Ion exchenge technology I (Springer).

Ma, Y., Wang, X., Wang, M., Jiang, C., Xiang, X., and Zhang, X. (2015). Separation of V(IV) and Fe(III) from the acid leach solution of stone coal by D2EHPA/TBP. Hydrometallurgy *153*, 38–45.

Manzano, R.V. (2017). Valorización de Cobre y Zinc Contenidos en Residuos Líquidos Industriales Mediante Integración de Tecnologías de Membrana e Intercambio Iónico. 56.

Matlock, M.M., Howerton, B.S., and Atwood, D.A. (2002). Chemical precipitation of heavy metals from acid mine drainage. Water Res. *36*, 4757–4764.

Mcbride, M.B. (1989). Advances in Soil Science.

Moskalyk, R.R., Alfantazi, A., Tombalakian, A.S., and Valic, D. (1999). Anode effects in electrowinning. Miner. Eng. *12*, 65–73.

Nikolic, N.D., and Popov, K.I. (2010). Hydrogen co-deposition effects on the structure of electrodeposited copper. In Modern Aspects of Electrochemistry, No.48: Electrodeposition. Theory and Practice, S.S. Djokic, and P.L. Cavalloti, eds. (London: Springer), pp. 251–291.

Panda, B., and Das, S.C. (2001). Electrowinning of copper from sulfate electrolyte in presence of sulfurous acid. Hydrometallurgy *59*, 55–67.

Park, K.H., Parhi, P.K., and Kang, N.H. (2012). Studies on Removal of Low Content Copper from the Sea Nodule Aqueous Solution using the Cationic Resin TP 207. Sep. Sci. Technol. *47*, 1531–1541.

Perez, N. (2004). Electrochemistry and Corrosion Science (Boston: Kluwer Academic Publishers).

Richardson, J.F., Harker, J.H., and Backhurst, J.R. (2002). Coulson and Richardson's Chemical Engineering (Oxford: Butterworth Heinemann).

Salles, R.C.M., De Oliveira, G.C.G., Díaz, S.L., Barcia, O.E., and Mattos, O.R. (2011). Electrodeposition of Zn in acid sulphate solutions: PH effects. Electrochim. Acta *56*, 7931–7939.

SenGupta, A.K. (2004). Ion Exchange and Solvent Extraction (New York: Marcel Dekker).

Shaabani, A., Teimouri, F., and Lee, D.G. (2003). Ion exchange catalysis in oxidation of organic compounds with KMnO4. Synth. Commun. *33*, 1057–1065.

Shackelford, B.C.D., Malusis, M.A., Majeski, M.J., Stern, R.T., and Member, A. (1999). Electrical Conductivity Breakthrough Curves. 260–270.

Simpson, C., and Laurie, S.H. (1999). Ion exchange studies on zinc-rich waste liquors. Hydrometallurgy *51*, 335–344.

Taute, J.J. (2013). Removal of Zinc from a Base-Metal Solution Using Ion Exchange at Rustenburg Base Metal Refiners. University of Cape Town.

Taute, J.J., Sole, K.C., and Hardwick, E. (2013). Zinc removal from a base metal solution by ion exchange : process design to full-scale operation. Base Met. Conf. 179–192.

UGT (2013). XVII Convenio Colectivo Nacional de Ingenieria y Oficinas de Estudios Técnicos. *2013*.

Valverde, J.L., de Lucas, A., Carmona, M., González, M., and Rodríguez, J.F. (2004). Equilibrium data of the exchange of Cu2+, Cd2+ and Zn2+ ions for H+ on the cathionic exchanger Lewatit TP-207. J. Chem. Technol. Biotechnol. *79*, 1371–1375.

Venkateswaran, K. V, Srinivasan, G.N., and Nandakumar, V. (1996). Electrowinning of zinc - Effect of metallic impurities and addition agents. Bull. Electrochem. *12*, 349–351.

Wei, X., Viadero, R.C., and Buzby, K.M. (2005). Recovery of Iron and Aluminum from Acid Mine Drainage by Selective Precipitation. Environ. Eng. Sci. *22*, 745–755.

Winiarski, J., Le, A., Pohl, P., and Szczygie, B. (2016). Surface & Coatings Technology The effect of pH of plating bath on electrodeposition and properties of protective ternary Zn – Fe – Mo alloy coatings. *299*, 81–89.

Younger, P.L., Banwart, S.A., and Hedin, R.S. (2002). Mine water.

Zhou, J., Wu, J., Liu, Y., Zou, F., Wu, J., Li, K., Chen, Y., Xie, J., and Ying, H. (2013). Modeling of breakthrough curves of single and quaternary mixtures of ethanol, glucose, glycerol and acetic acid adsorption onto a microporous hyper-cross-linked resin. Bioresour. Technol. *143*, 360–368.

Zoski, C.G. (2007). Handbook of electrochemistry (Amsterdam: Elsevier B.V.).

Spain | Sigma-Aldrich.

Kinesis | Specialists in the supply and support of Chromatography Consumables.